Monthly Notices
of the
ROYAL ASTRONOMICAL SOCIETY

Mon. Not. R. Astron. Soc. **401,** 479–499 (2010) doi:10.1111/j.1365-2966.2009.15664.x

Wind-driving protostellar accretion discs – I. Formulation and parameter constraints

Arieh Königl,[1⋆] Raquel Salmeron[2⋆] and Mark Wardle[3⋆]

[1]*Department of Astronomy & Astrophysics and The Enrico Fermi Institute, The University of Chicago, Chicago, IL 60637, USA*
[2]*Research School of Astronomy & Astrophysics and Research School of Earth Sciences, The Australian National University, Canberra ACT 0200, Australia*
[3]*Department of Physics and Engineering, Macquarie University, Sydney NSW 2109, Australia*

Accepted 2009 September 3. Received 2009 September 3; in original form 2009 April 20

ABSTRACT

We study a model of weakly ionized, protostellar accretion discs that are threaded by a large-scale, ordered magnetic field and power a centrifugally driven wind. We consider the limiting case where the wind is the main repository of the excess disc angular momentum and generalize the radially localized disc model of Wardle & Königl, which focused on the ambipolar diffusion regime, to other field diffusivity regimes, notably Hall and Ohm. We present a general formulation of the problem for nearly Keplerian, vertically isothermal discs using both the conductivity-tensor and the multifluid approaches and simplify it to a normalized system of ordinary differential equations in the vertical space coordinate. We determine the relevant parameters of the problem and investigate, using the vertical-hydrostatic-equilibrium approximation and other simplifications, the parameter constraints on physically viable solutions for discs in which the neutral particles are dynamically well coupled to the field already at the mid-plane. When the charged particles constitute a two-component ion–electron plasma, one can identify four distinct sub-regimes in the parameter domain where the Hall diffusivity dominates and three sub-regimes in the Ohm-dominated domain. Two of the Hall sub-regimes can be characterized as being ambipolar diffusion-like and two as being Ohm-like: the properties of one member of the first pair of sub-regimes are identical to those of the ambipolar diffusion regime, whereas one member of the second pair has the same characteristics as one of the Ohm sub-regimes. All the Hall sub-regimes have $B_{r\mathrm{b}}/|B_{\phi\mathrm{b}}|$ (ratio of radial-to-azimuthal magnetic field amplitudes at the disc surface) >1, whereas in two Ohm sub-regimes this ratio is <1. When the two-component plasma consists, instead, of positively and negatively charged grains of equal mass, the entire Hall domain and one of the Ohm sub-regimes with $B_{r\mathrm{b}}/|B_{\phi\mathrm{b}}| < 1$ disappear. All viable solutions require the mid-plane neutral–ion momentum exchange time to be shorter than the local orbital time. We also infer that vertical magnetic squeezing always dominates over gravitational tidal compression in this model. In a follow-up paper we will present exact solutions that test the results of this analysis in the Hall regime.

Key words: accretion, accretion discs – MHD – stars: formation – ISM: jets and outflows.

1 INTRODUCTION

Star formation is thought to be induced by the gravitational collapse of the dense cores of molecular clouds (e.g. Shu, Adams & Lizano 1987). During the collapse, angular momentum conservation results in the progressive increase of the centrifugal force, a process that eventually halts the infalling matter and leads to the development of a central mass (protostar) surrounded by a rotationally supported, gaseous disc. In the presence of an angular momentum transport mechanism, mass accretion on to the protostar proceeds through this disc, and it is believed that this is how stars typically gain most of their mass.

A common feature of accreting protostellar systems is their association with energetic bipolar outflows that propagate along the rotation axis of the source (e.g. Bally, Reipurth & Davis 2007). The outflows from low-bolometric-luminosity objects ($L_{\mathrm{bol}} < 10^3\,\mathrm{L}_\odot$) have velocities in the range $\sim$150–400 km s^{-1} (of the order of the escape speed from the vicinity of the central protostar) and are typically well collimated (opening half-angles $\sim3^\circ$–5° on scales of 10^3–10^4 au). The connection between accretion discs and

⋆E-mail: arieh@jets.uchicago.edu (AK); raquel@mso.anu.edu.au (RS); wardle@physics.mq.edu.au (MW)

outflows, which extends smoothly from very low-mass stars and brown dwarfs (e.g. Mohanty, Jayawardhana & Basri 2005) all the way up to protostars with masses of at least $\sim 10\,M_\odot$ (e.g. Corcoran & Ray 1998), is manifested by the observed correlations between accretion diagnostics (e.g. inverse P-Cygni profiles and excess emission in UV, IR and millimetre wavelengths) and outflow signatures (e.g. P-Cygni profiles, optical forbidden lines, thermal radio radiation and the presence of molecular lobes) in these objects (e.g. Hartigan, Edwards & Ghandour 1995). Also relevant are the correlations of the type $\dot{M} \propto L_{\rm bol}^{\delta}$ (with $\delta \sim 0.6$–0.7) that have been inferred for both accretion and outflow rates in low- and high-$L_{\rm bol}$ objects (e.g. Levreault 1988) and the joint decline in outflow activity and disc frequency (as well as in the inferred accretion rate) with stellar age (e.g. Calvet, Hartmann & Strom 2000; Calvet et al. 2005).

These features point to an underlying physical link between accretion and outflow processes in these systems. A natural explanation for this connection is that outflows provide an efficient means of transporting away the excess angular momentum and of tapping the liberated gravitational potential energy of the accreted matter. In this scenario, disc material is centrifugally accelerated by the torque exerted by a large-scale, ordered magnetic field that threads the disc (Blandford & Payne 1982, hereafter BP82; see also the reviews by Königl & Pudritz 2000; Pudritz et al. 2007; Königl & Salmeron 2009). A dynamically significant, ordered field component is indicated by the hourglass field morphology detected by polarization measurements in several pre-collapse molecular cloud cores on subparsec scales (e.g. Schleuning 1998; Girart, Rao & Marrone 2006; Kirby 2009). These interstellar field lines are expected to be advected inward when the core undergoes gravitational collapse and could naturally give rise to an ordered field in the resulting protostellar discs. Alternatively, an ordered field component could be generated locally in the disc (and star) by a dynamo process. The comparatively high momentum discharges inferred in protostellar outflow sources are consistent with this interpretation, as alternative wind-driving mechanisms would fall far short of the indicated requirements (e.g. Königl & Pudritz 2000). The centrifugal wind picture can also naturally account for the comparatively high ratio ($\sim$0.1) of the mass outflow to the mass accretion rate that is inferred in both the quiescent and the outburst phases of low-mass protostars (e.g. Hartmann & Kenyon 1996; Ray et al. 2007).

Vertical angular-momentum transport by a large-scale, ordered magnetic field is expected to dominate radial angular-momentum transport via turbulence induced by the magnetorotational instability (MRI; e.g. Balbus & Hawley 1998) when the disc is threaded by a comparatively strong magnetic field, corresponding to the ratio a_0 of the Alfvén speed $v_{\rm A0}$ (where the subscript 0 denotes the mid-plane) to the isothermal sound speed $c_{\rm s}$ being not much smaller than unity.[1] When this condition is satisfied, angular momentum transport by a small-scale, disordered magnetic field is suppressed because the wavelength of the most unstable MRI perturbations exceeds the magnetically reduced disc scaleheight (e.g. Wardle & Königl 1993, hereafter WK93). On the other hand, when the magnetic field is comparatively weak ($a_0 \ll 1$), MRI-induced radial transport should dominate.

[1] Note that vertical angular-momentum transport can also be mediated by additional mechanisms (not considered in this paper), including magnetic braking (the launching of torsional Alfvén waves into the ambient interstellar medium; e.g. Krasnopolsky & Königl 2002), 'failed' winds (which do not become supersonic or super-Alfvénic) and non-steady phenomena.

Previous studies have considered the aforementioned radial and vertical angular-momentum transport mechanisms under a number of simplifying assumptions. The MRI has been analyzed in both its linear and non-linear stages (e.g. Sano & Stone 2002a,b; Salmeron & Wardle 2003, 2005; Fleming & Stone 2003; Desch 2004; Sano et al. 2004; Turner, Sano & Dziourkevitch 2007). Similarly, centrifugal wind-driving discs have been examined both semi-analytically, making use of self-similarity formulations (e.g. WK93; Li 1995, 1996; Ferreira 1997), and through numerical simulations that utilize resistive-MHD codes (e.g. Casse & Keppens 2002; Kuwabara et al. 2005; Meliani, Casse & Sauty 2006; Zanni et al. 2007). It is, however, likely that both the radial and vertical modes of angular momentum transport play a role in real accretion discs. While quasi-steady disc models in which both mechanisms operate had been considered in the literature (e.g. Lovelace, Romanova & Newman 1994; Casse & Ferreira 2000; Ogilvie & Livio 2001), they did not specifically link the radial transport of angular momentum with its origin in MRI-induced turbulence. In a first attempt in this direction, Salmeron, Königl & Wardle (2007) explored the possibility that radial and vertical transport could operate at the same radial location in a protostellar disc. They derived an approximate criterion for identifying the vertical extent of a wind-driving disc at the given radius that is unstable to MRI-induced turbulence and obtained a quantitative estimate (based on the numerical simulations of Sano et al. 2004) of the amount of angular momentum that is removed radially from that region.

An important consideration for the analysis of magnetic angular momentum transport in protostellar discs is that these discs are generally weakly ionized over most of their extents, so magnetic diffusivity effects are significant. This is a critical issue because both the centrifugal-wind and MRI-turbulence transport mechanisms require a minimum level of field–matter coupling to be effective. A complete model therefore needs to take into account the detailed ionization and conductivity structure of the disc/wind system. At low densities (near the disc surfaces and at large radii), the disc is typically in the *ambipolar diffusion* regime. As the density and the shielding column increase (closer to the disc mid-plane and the central source), the fluid passes successively through the *Hall* and *Ohm* diffusivity regimes (see Section 2). Note, however, that the disc parameters may well be such that the gas does not clearly correspond to any one of these limiting cases and must instead be described more generally using either the conductivity-tensor (Section 2.1) or the multifluid-decomposition (Section 3.14) formulations. Most previous treatments have simplified the problem by focusing on a single conductivity regime. In particular, WK93 and Salmeron et al. (2007) concentrated on the ambipolar diffusion limit (although WK93 also discussed the Hall-current effects). WK93 were able to obtain simple analytic constraints on the parameter values for physically viable wind-driving disc solutions in this limit by modelling the vertical structure of the disc under the *hydrostatic* (negligible vertical velocity) approximation. One of their derived constraints yielded the minimum required degree of field–matter coupling, and they proceeded to verify their analysis by obtaining numerical solutions for discs in this *strong coupling* regime.

Although it is in principle possible to seek a self-similar solution for the global disc/wind configuration (e.g. Königl 1989; Ferreira 1997), WK93 adopted a somewhat simpler approach in which they obtained a solution for the vertical structure of a radially localized (radial extent $\Delta r \ll r$ at a cylindrical radius r) region of the disc and matched it to a self-similar (in the spherical radial coordinate R) global wind solution of the type originally constructed by BP82.

This approach facilitated the derivation of viability and consistency constraints involving exclusively the disc model parameters, and subsequently Li (1996) demonstrated that the basic features of this solution are consistent with those of a fully global disc/wind similarity solution. Our aim in this paper is to generalize the parameter constraints derived in WK93 for the ambipolar diffusion regime to the other basic diffusivity regimes, namely Hall and Ohm. In each of the latter regimes, we identify parameter combinations that yield different sets of constraints, which correspond to solutions with distinct physical properties, and we use these constraints to delineate the Hall and Ohm sub-regimes in parameter space where one can derive viable, strongly coupled, wind-driving disc solutions. In a follow-up paper (Salmeron et al., in preparation, hereafter Paper II) we test the results for the Hall regime – derived by using the hydrostatic approximation – against full numerical solutions obtained in the radially localized disc approximation of WK93.

As noted above, the Hall and Ohm diffusivity regimes are likely to apply near the mid-plane in the inner regions of real protostellar discs. Typically, the surface regions from which the wind is driven would be sufficiently well ionized by cosmic rays and by the protostellar radiation field (see Section 2.1) to lie in the ambipolar diffusion regime (e.g. Salmeron & Wardle 2005; Königl & Salmeron 2009). Nevertheless, we adopt the approximation that the entire disc cross-section between the mid-plane and the base of the wind lies in a single diffusivity sub-regime in order to bring out the distinct properties of the solutions for each parameter range. This approximation is less appropriate for the Ohm regime, both because *two* additional regimes (ambipolar diffusion *and* Hall) would be encountered on the way up to the disc surface in this case and because the column densities of wind-driving discs are relatively small (especially in comparison with those typically implied by radial-turbulent-transport models) and are therefore likely to contain only limited regions (if any at all) where the Ohm diffusivity dominates. We have nevertheless chosen to include the Ohm regime in our analysis of weakly ionized discs for completeness as well as for possible comparisons with resistive-MHD numerical simulations.[2] The results of this analysis could potentially be applicable also to the collisionally ionized innermost region of the disc, where anomalous resistivity (the enhanced drag between ions and electrons due to scattering off electromagnetic waves generated by current-driven plasma instabilities) might develop. To obtain explicit solutions in the different diffusivity regimes, we have generalized the WK93 model setup by implementing a conductivity-tensor scheme that can be applied to any given vertical ionization structure. In Paper II, we use a simplified version of this scheme to mimic the single-diffusivity conditions adopted in the present work.

This paper is organized as follows. Section 2 summarizes the formulation, including the disc model and the governing equations. Section 3 describes the methodology we employ to reduce these equations to a set of ordinary differential equations (ODEs) in the vertical coordinate z and to express them in a dimensionless form; it also lists the parameters of the problem. Section 4 derives the constraints that characterize the parameter space where physically viable solutions exist and explicates them for the Hall regime, with the corresponding constraints for the Ohm regime presented in Section 5. The key findings of the paper are discussed in Section 6 and summarized in Section 7.

[2] Note, however, that we do not continue to consider this case in Paper II, which concentrates on the ambipolar-diffusion and Hall regimes.

2 FORMULATION

2.1 Disc model

We model the disc as being in a steady state, geometrically thin, vertically isothermal, nearly Keplerian and in dynamical equilibrium in the gravitational potential of the central protostar. Since we expect all the physical variables to exhibit smooth spatial variations, the assumption of geometrical thinness enables us to neglect the radial derivative terms ($|\partial/\partial r| \sim 1/r$) in our equations in comparison with the vertical derivative terms ($|\partial/\partial z| \sim 1/h$), where r and z are cylindrical coordinates and $h(r)$ ($\ll r$) is the disc pressure (or density) scaleheight at the radius r.[3] The disc material is assumed to be weakly ionized, with the abundances of charged species being so low that (i) the effect of ionization and recombination processes on the neutral gas can be neglected and (ii) the inertial, gravitational and thermal forces on the ionized species are negligible in comparison with the electromagnetic force exerted by a large-scale, ordered magnetic field. Under these approximations, separate equations of motion for the charged species are not required, and their effect on the neutrals can be incorporated via a conductivity tensor $\boldsymbol{\sigma}$ (e.g. Cowling 1976; Wardle 1999 and references therein), which is a function of position $\{r, z\}$. This formulation makes it possible to systematically include different ionized fluid components as well as the three basic field–matter diffusion mechanisms (ambipolar, Hall and Ohm). The conductivity-tensor components are the Ohm, Hall and Pedersen terms, given by

$$\sigma_{\rm O} = \frac{ec}{B} \sum_j n_j |Z_j| \beta_j, \tag{1}$$

$$\sigma_{\rm H} = \frac{ec}{B} \sum_j \frac{n_j Z_j}{1+\beta_j^2} \tag{2}$$

and

$$\sigma_{\rm P} = \frac{ec}{B} \sum_j \frac{n_j |Z_j| \beta_j}{1+\beta_j^2}, \tag{3}$$

respectively (e.g. Wardle & Ng 1999). In the above expressions, n_j is the number density of charged species j (of mass m_j and total electric charge $Z_j e$), c is the speed of light and

$$\beta_j = \frac{|Z_j| eB}{m_j c} \frac{1}{\gamma_j \rho} \tag{4}$$

is the Hall parameter, the ratio of the gyrofrequency and the collision frequency of species j with the neutrals, which measures the relative importance of the Lorentz and drag forces on the motion of the charged species. In these equations,

$$B \equiv |\mathbf{B}| \, {\rm sgn}\{B_z\} \tag{5}$$

is the *signed* magnetic field amplitude, with the sign introduced to keep the dependence of the Hall conductivity on the magnetic field polarity.[4] Also, in equation (4),

$$\gamma_j = \frac{\langle \sigma v \rangle_j}{m_j + m}, \tag{6}$$

[3] The only exception to this approach is our retention of the radial derivative of the azimuthal velocity component v_ϕ (see WK93).

[4] Note from equations (1)–(3) that, in contrast with $\sigma_{\rm H}$, which depends on an odd power of B, both the Ohm and Pedersen conductivities are independent of the magnetic field polarity.

where $m = 2.33\, m_{\rm H}$ is the mean mass of the neutral particles in terms of the hydrogen nucleus mass $m_{\rm H}$, ρ is the density of the neutral gas and $\langle \sigma\ v\rangle_j$ is the rate coefficient of momentum exchange of species j with the neutrals.

The above equations can be used to treat charged species with a wide range of masses and degrees of coupling with the neutral gas. However, to simplify the analysis and make it more transparent, we henceforth specialize to a fluid with only two charged species, one with positive charge (which we refer to as 'ions' and denote by a subscript 'i'; $Z_{\rm i} > 0$) and the other with negative charge ('electrons,' subscript 'e', satisfying $Z_{\rm e} < 0$). This description is a good approximation both in the comparatively low-density regions of protostellar discs, where the two species can be taken as metal ions (of typical mass $m_{\rm i} = 30\, m_{\rm H}$; e.g. Draine, Roberge & Dalgarno 1983) and electrons, and in high-density ($\rho \gtrsim 10^{-13}$ g cm^{-3}) regions where the dominant charge carriers are positively and negatively charged dust grains of equal mass (e.g. Umebayashi & Nakano 1990; Neufeld & Hollebach 1994; Krasnopolsky & Königl 2002).[5] The 'ion' and 'electron' Hall parameters are related by $\beta_{\rm i} = q\beta_{\rm e}$, where

$$q = \frac{m_{\rm e}}{m_{\rm i}}\,\frac{m_{\rm i}+m}{m_{\rm e}+m}\,\frac{\langle\sigma v\rangle_{\rm e}}{\langle\sigma v\rangle_{\rm i}}. \tag{7}$$

In the case of charged grains of equal and opposite charge as well as equal mass, $q = 1$, whereas in the case of ions and electrons we find, using

$$\langle\sigma v\rangle_{\rm i} = 1.6\times10^{-9}\,{\rm cm^3\,s^{-1}} \tag{8}$$

and

$$\langle\sigma v\rangle_{\rm e} \approx (1\times10^{-15}\,{\rm cm^2})\left(\frac{128kT}{9\pi m_{\rm e}}\right)^{1/2} \tag{9}$$

from the results of Draine et al. (1983), that $q \approx 1.3\times10^{-4}\sqrt{T}$ (where T denotes the gas temperature and k is Boltzmann's constant). In our analysis, we often encounter the product $s \equiv \beta_{\rm e}\,\beta_{\rm i} = \beta_{\rm i}^2/q$, which is sometimes referred to in the literature as the *ion slip factor* (e.g. Mitchner & Kruger 1973).

With the help of the charge-neutrality condition,

$$\sum_j n_j Z_j = 0\,, \tag{10}$$

equations (1)–(3) become

$$\sigma_{\rm O} = \frac{cen_{\rm e}|Z_{\rm e}|}{B}(\beta_{\rm e}+\beta_{\rm i}), \tag{11}$$

$$\sigma_{\rm H} = \frac{cen_{\rm e}|Z_{\rm e}|}{B}\,\frac{(\beta_{\rm e}+\beta_{\rm i})(\beta_{\rm e}-\beta_{\rm i})}{\left(1+\beta_{\rm e}^2\right)\left(1+\beta_{\rm i}^2\right)} \tag{12}$$

and

$$\sigma_{\rm P} = \frac{cen_{\rm e}|Z_{\rm e}|}{B}\,\frac{(1+\beta_{\rm i}\beta_{\rm e})(\beta_{\rm e}+\beta_{\rm i})}{\left(1+\beta_{\rm e}^2\right)\left(1+\beta_{\rm i}^2\right)}, \tag{13}$$

respectively (e.g. Salmeron & Wardle 2003). We also make use of $\sigma_\perp = \sqrt{\sigma_{\rm H}^2+\sigma_{\rm P}^2}$, the total conductivity perpendicular to the magnetic field, which is given by

$$\sigma_\perp = \frac{cen_{\rm e}|Z_{\rm e}|}{B}\,\frac{(\beta_{\rm e}+\beta_{\rm i})}{\left[\left(1+\beta_{\rm e}^2\right)\left(1+\beta_{\rm i}^2\right)\right]^{1/2}}. \tag{14}$$

[5] During the late ($\gtrsim 10^5$ yr) phases of protostellar evolution, after the dust has largely settled to the mid-plane (e.g. Nakagawa, Nakazawa & Hayashi 1981; Dullemond & Dominik 2004; D'Alessio et al. 2006), ions and electrons could dominate the charged species also in the dense inner regions of the disc.

The ratios of the conductivity-tensor components $\sigma_{\rm H}$, $\sigma_{\rm P}$ and $\sigma_{\rm O}$ determine the relative importance of the ambipolar, Hall and Ohm diffusion mechanisms (e.g. Wardle & Ng 1999). These ratios, in turn, depend on the magnitudes of the 'ion' and 'electron' Hall parameters, which are functions of the neutral density and magnetic field amplitude. The spatial variation of the latter quantities in protostellar systems results in different diffusion mechanisms dominating in different regions of the disc. We now briefly outline the main properties of these different regimes, although it must be borne in mind that some regions of the disc will inevitably correspond to the transition zones between two such regimes (or between any of the sub-regimes that we identify) and hence cannot be so simply classified.

(i) *Ambipolar diffusion*. This regime dominates when $\sigma_{\rm O} \gg \sigma_{\rm P} \gg |\sigma_{\rm H}|$ or, equivalently, when $|\beta_{\rm i}| \gg 1$. In this case the magnetic field is effectively frozen into the ionized fluid component (the 'electrons' and the 'ions') and drifts with it through the neutrals. This regime is expected to dominate at relatively low densities in protostellar discs – throughout the vertical column in the outermost regions of the disc (e.g. WK93) and close to the disc surfaces at smaller radii.

(ii) *Hall diffusion* ($\sigma_{\rm P} \ll |\sigma_{\rm H}| \ll \sigma_{\rm O}$). These conditions are satisfied when the most highly mobile charged particles (having the highest value of $|Z_j e/m_j|$ – the electrons in the case of an ion–electron plasma) are well coupled to the magnetic field ($|\beta_{\rm e}| \gg 1$) even as the drift of the more massive charged particles of the opposite sign (i.e. the ions in an ion–electron plasma) through the neutrals is strongly inhibited by collisions ($|\beta_{\rm i}| \ll 1$). In this limit, the current in an ion–electron plasma is dominated by the electrons, which drift perpendicularly to the magnetic and electric fields (thereby minimizing the electromagnetic force acting on them, with the electron–neutral drag force usually remaining negligible). This gives rise to the Hall current, which is perpendicular to both the electric and magnetic fields. This regime typically dominates close to the disc mid-plane on 'intermediate' radial scales (e.g. Li 1996; Wardle 1999; Sano & Stone 2002a; Salmeron & Wardle 2005). Note that $\sigma_{\rm H}$ (and therefore the Hall diffusivity regime) vanishes identically when $|\beta_{\rm i}| = |\beta_{\rm e}|$ (i.e. when $q = 1$).

(iii) *Ohm diffusion* ($\sigma_{\rm O} \approx \sigma_{\rm P} \gg |\sigma_{\rm H}|$ or, equivalently, $|\beta_{\rm e}| \ll 1$). In this case all the ionized species are uncoupled from the field by collisions with the neutrals, so the magnetic field cannot be regarded as being frozen into any of the fluid components. In this parameter regime one can formulate the problem in terms of a simple scalar conductivity, corresponding to the familiar ohmic resistivity. However, as we show in Section 5, one cannot in general neglect the Hall term in Ohm's law in classifying the physically viable disc solutions in this regime. The Ohm diffusivity may dominate in the most shielded inner regions of particularly massive protostellar discs (but outside the radius where collisional ionization of alkali metals sets in). As we noted in Section 1, it is also conceivable that *anomalous* Ohm diffusivity dominates in the collisionally ionized zone further in. In fact, certain models (e.g. Bell & Lin 1994; Gammie 1999) link the formation of a higher ionization zone in the innermost region of the disc to the development of FU Orionis-type outbursts, during which most of the accretion on to the central protostar may take place (e.g. Calvet et al. 2000).

Note that the ion slip factor $s = \beta_{\rm i}^2/q$ is $\gg 1$ in the ambipolar diffusion regime and $\ll 1$ in the Ohm regime. This factor can be either <1 or >1 for a $q \ll 1$ two-component plasma in the Hall regime. This suggests that in the latter case one can distinguish between the ambipolar diffusion-modified Hall regime, in which the

inequalities $\sqrt{q} \ll |\beta_i| \ll 1$ are satisfied, and the Ohm diffusion-modified Hall regime, in which the inequalities $q \ll |\beta_i| \ll \sqrt{q}$ are obeyed (Königl 1997). We return to provide explicit support for this characterization in Section 6.

In the fiducial minimum-mass solar nebula model (Hayashi 1981), the ambipolar, Hall and Ohm diffusivity regimes dominate at the disc mid-plane on scales $r \gtrsim 10$ au, ∼1–10 au and ∼0.1–1 au, respectively, for likely magnetic field strengths and when the effect of grains is neglected. If sufficiently small ($\lesssim 0.1$ μm) grains are present at $z = 0$ and the density is large enough that they carry a significant fraction of both the negative *and* the positive charges then the extent of the mid-plane Hall regime is strongly reduced (e.g. Wardle & Ng 1999; Wardle 2007; Salmeron & Wardle 2008). Wind-driving accretion-disc models typically have lower column densities and mid-plane densities than either the minimum-mass model or standard viscous disc models (a reflection of their comparatively high inward drift speeds; see Section 6): this has the effect of pushing both the inner and outer edges of the mid-plane Hall regime inward. In practice, the spatial distribution of the different diffusivity regimes depends on the mass accretion rate, the dust content and the nature of the ionization mechanisms that affect the disc, and it could vary from source to source and during the evolution of any particular system.

Evaluating the conductivity tensor in a real disc involves calculating the ionization balance and associated abundances of charged species at any given location. This balance is, in turn, the result of a delicate equilibrium between ionization and recombination processes acting both in the gas phase and on the surfaces of dust grains (if present). The most relevant ionization sources outside the central ∼0.1 au of the disc are non-thermal: X-rays and UV radiation, emanating from the magnetically active young star and its magnetosphere, as well as interstellar cosmic rays and radioactive decay inside the disc (e.g. Hayashi 1981; Umebayashi & Nakano 1981, 1990; Igea & Glassgold 1999). In the vicinity of the star, the disc surface is ionized mainly by X-rays, but UV radiation also becomes important at larger distances (e.g. Semenov, Wiebe & Henning 2004; Alexander, Clarke & Pringle 2005; Glassgold et al. 2005). Within the innermost ∼0.1 au the degree of ionization could be significantly raised by collisional ionization of alkali metals, particularly potassium (e.g. Gammie 1996; Li 1996). A detailed calculation of the vertical ionization and conductivity structure of a wind-driving disc has so far been performed only in the context of a radially localized treatment and without including dust (e.g. Königl & Salmeron 2009); a generalization to a global disc/wind model and the incorporation of dust remain to be done.

In this paper and in Paper II, we adopt a simpler treatment than the one outlined above, motivated by the fact that our main interest is to (i) identify the regions in parameter space where viable wind-driving disc solutions can be found under weak-ionization conditions and (ii) derive the main properties of these solutions. As our classification scheme requires the specification, at the mid-plane of the disc, of the values of three distinct variables (see Section 6), we make the assumption that the density and ionization structure of the disc is such that, at the radial location under consideration, the parameter regime determined by the mid-plane values of the chosen three variables continues to apply throughout the vertical extent of the disc. In the analysis presented in Sections 4 and 5 of this paper, we use the variables β_e, β_i and Υ, the neutral–ion coupling parameter defined in equation (82), and assume that they remain constant with height at least within the quasi-hydrostatic layer. In the numerical work presented in Paper II, we choose the distinct variables to be two independent ratios of the conductivity-tensor components and the field–matter coupling parameter Λ (the Elsasser number; see Section 3.13), and we assume that they remain constant between $z = 0$ and the sonic point above the disc surface. Notwithstanding the difference in the specific variables chosen in each case, these two procedures are effectively equivalent.

2.2 Governing equations

Our basic equations describe the conservation of mass

$$\frac{\partial \rho}{\partial t} + \nabla \cdot (\rho \boldsymbol{v}) = 0 \tag{15}$$

and momentum

$$\frac{\partial \boldsymbol{v}}{\partial t} + (\boldsymbol{v} \cdot \nabla)\boldsymbol{v} + \frac{1}{\rho}\nabla P + \nabla\Phi - \frac{\boldsymbol{J}\times\boldsymbol{B}}{c\rho} = 0 \tag{16}$$

for the neutral gas, as well as the evolution of the magnetic field

$$\frac{\partial \boldsymbol{B}}{\partial t} = \nabla\times\boldsymbol{E} = \nabla\times(\boldsymbol{v}\times\boldsymbol{B}) - c\nabla\times\boldsymbol{E}', \tag{17}$$

where $\boldsymbol{v}$ is the fluid velocity and $\boldsymbol{J}$ is the current density. In the equation of motion (equation 16)

$$P = \rho c_s^2 = \frac{\rho k T}{\mu m_H} \tag{18}$$

is the gas pressure, c_s is the isothermal sound speed and $\mu \equiv m/m_H = 2.33$ is the molecular weight. In addition, Φ is the gravitational potential of the central object, given by

$$\Phi = -\frac{GM}{(r^2 + z^2)^{1/2}}, \tag{19}$$

where G is the gravitational constant and M is the mass of the protostar (which is treated as a point mass at the origin of the coordinate system). Note that in equation (16) we have made use of the low-inertia limit for the ionized species by balancing the sum of the ion–neutral and electron–neutral drag forces ($\boldsymbol{f}_{in}$ and $\boldsymbol{f}_{en}$, respectively) by the Lorentz force,

$$\boldsymbol{f}_{in} + \boldsymbol{f}_{en} = \frac{\boldsymbol{J}\times\boldsymbol{B}}{c}, \tag{20}$$

on the assumption that all other terms in the momentum equations for the charged particles remain small.

In the induction equation (17)

$$\boldsymbol{E}' = \boldsymbol{E} + \frac{\boldsymbol{v}\times\boldsymbol{B}}{c} \tag{21}$$

is the electric field in the frame comoving with the neutrals and $\boldsymbol{E}$ is the corresponding field in the inertial (laboratory) frame. The field $\boldsymbol{E}'$ is related to the current density $\boldsymbol{J}$ through the conductivity tensor $\boldsymbol{\sigma}$ (see equation 24). Furthermore, the magnetic field satisfies the solenoidal condition

$$\nabla \cdot \boldsymbol{B} = 0, \tag{22}$$

which implies (in analogy with the inference on ρv_z following equation 35) that in a thin disc B_z is approximately constant with height, whereas the current density obeys Ampère's law

$$\boldsymbol{J} = \frac{c}{4\pi}\nabla\times\boldsymbol{B} \tag{23}$$

(where we neglected the displacement current) and Ohm's law,

$$\boldsymbol{J} = \boldsymbol{\sigma}\cdot\boldsymbol{E}' = \sigma_O\boldsymbol{E}'_\parallel + \sigma_H\hat{\boldsymbol{B}}\times\boldsymbol{E}'_\perp + \sigma_P\boldsymbol{E}'_\perp, \tag{24}$$

where $\hat{\boldsymbol{B}}$ is the unit vector in the direction of $\boldsymbol{B}$.

Equation (24) can be inverted to yield the following expression for $\boldsymbol{E}'$:

$$\boldsymbol{E}' = \frac{\boldsymbol{J}}{\sigma_{\rm O}} + \frac{\sigma_{\rm H}}{\sigma_\perp^2}\frac{\boldsymbol{J}\times\boldsymbol{B}}{B} - \left(\frac{\sigma_{\rm P}}{\sigma_\perp^2} - \frac{1}{\sigma_{\rm O}}\right)\frac{(\boldsymbol{J}\times\boldsymbol{B})\times\boldsymbol{B}}{B^2}. \tag{25}$$

The terms on the right-hand side of equation (25) are, from left to right, the resistive (Ohm), Hall and ambipolar diffusion contributions, respectively. Substituting equations (11)–(14) for a two-component plasma into equation (25) gives

$$\boldsymbol{E}' = \frac{\beta_{\rm e}}{\beta_{\rm e}+\beta_{\rm i}}\frac{\boldsymbol{J}}{\sigma_{\rm e}} + \frac{\beta_{\rm e}-\beta_{\rm i}}{\beta_{\rm e}+\beta_{\rm i}}\frac{\boldsymbol{J}\times\boldsymbol{B}}{cen_{\rm e}|Z_{\rm e}|} - \frac{\beta_{\rm e}\beta_{\rm i}}{\beta_{\rm e}+\beta_{\rm i}}\frac{(\boldsymbol{J}\times\boldsymbol{B})\times\boldsymbol{B}}{Bcen_{\rm e}|Z_{\rm e}|}, \tag{26}$$

where $\sigma_{\rm e}$ is the 'electron' electrical conductivity,

$$\sigma_{\rm e} = \frac{n_{\rm e}e^2Z_{\rm e}^2}{m_{\rm e}\gamma_{\rm e}\rho}. \tag{27}$$

Using $\beta_{\rm i}/(Bcen_{\rm e}|Z_{\rm e}|) = (c^2\gamma_{\rm i}\rho\rho_{\rm i})^{-1}$ in the last term of equation (26) and taking the limit $q \ll 1$ lead to

$$\boldsymbol{E}' = \frac{\boldsymbol{J}}{\sigma_{\rm e}} + \frac{\boldsymbol{J}\times\boldsymbol{B}}{cen_{\rm e}|Z_{\rm e}|} - \frac{(\boldsymbol{J}\times\boldsymbol{B})\times\boldsymbol{B}}{c^2\gamma_{\rm i}\rho_{\rm i}\rho}, \tag{28}$$

which is similar in form to expressions obtained in multifluid formulations (e.g. Königl 1989; Balbus & Terquem 2001).

The impact of the magnetic diffusivity on the evolution of the fluid can be more readily appreciated if we use the Ohm, Hall and ambipolar *diffusivity* terms, given by

$$\eta_{\rm O} = \frac{c^2}{4\pi\sigma_{\rm O}}, \tag{29}$$

$$\eta_{\rm H} = \frac{c^2}{4\pi\sigma_\perp}\frac{\sigma_{\rm H}}{\sigma_\perp} \tag{30}$$

and

$$\eta_{\rm A} = \frac{c^2}{4\pi\sigma_\perp}\frac{\sigma_{\rm P}}{\sigma_\perp} - \eta_{\rm O}. \tag{31}$$

Expressing the conductivity terms in equation (25) as functions of the Ohm, Hall and ambipolar diffusivities (equations 29–31) and substituting the resulting expression for $\boldsymbol{E}'$ into equation (17) leads to the following form of the induction equation (Wardle 2007):

$$\frac{\partial\boldsymbol{B}}{\partial t} = \nabla\times(\boldsymbol{v}\times\boldsymbol{B}) - \nabla\times[\eta_{\rm O}\nabla\times\boldsymbol{B} + \eta_{\rm H}(\nabla\times\boldsymbol{B})\times\hat{\boldsymbol{B}} + \eta_{\rm A}(\nabla\times\boldsymbol{B})_\perp], \tag{32}$$

where the subscript $\perp$ again denotes the direction perpendicular to $\boldsymbol{B}$. In the limit of a two-component plasma with $q \ll 1$, it can be shown (Wardle 2007) that

$$\eta_{\rm H} = \beta_{\rm e}\eta_{\rm O} \tag{33}$$

and

$$\eta_{\rm A} = \beta_{\rm e}\beta_{\rm i}\eta_{\rm O}\,. \tag{34}$$

Under ideal-MHD conditions all the magnetic diffusivity terms in the induction equation tend to zero and the evolution of the magnetic field is fully determined by the inductive term (the first term on the right-hand side of equations 17 and 32).

3 METHODOLOGY

3.1 Simplification of the equations

We now proceed to reduce the system of equations (15)–(17) and (23) to a set of ODEs in z. We closely follow the approach of WK93 and consider, as in that paper, a radially localized region of the disc that is threaded by an open magnetic field with an 'even' symmetry ($B_{r0} = B_{\phi 0} = 0$). Sections 3.2–3.8 deal with the mass and momentum conservation equations for the neutral gas and with the induction equation that describes the evolution of the magnetic field. Sections 3.9 and 3.10 are concerned with Ampère's and Ohm's laws, respectively.

3.2 Continuity

We are looking for steady-state ($\partial/\partial t = 0$), axisymmetric ($\partial/\partial\phi = 0$) solutions. In this limit, the continuity equation (15) reads

$$\frac{1}{r}\frac{\partial}{\partial r}(r\rho v_r) + \frac{\partial}{\partial z}(\rho v_z) = 0. \tag{35}$$

This expression is further simplified by neglecting the radial derivative term (see Section 2.1), which implies that ρv_z is constant with height. This approximation, first adopted in WK93, has been critiqued (e.g. Ferreira 1997) for not allowing v_z to assume negative values within the disc, as it must do in cases (expected to be typical) in which the disc thickness decreases as the protostar is approached. This issue can be fully addressed only in the context of a global disc/wind model. However, it can be expected that any error introduced by this approximation would be minimized if the upward mass flux remained small enough for v_z to have only a weak effect on the behaviour of the other variables within the disc. Under the assumption that $|v_r|$ is of the same order of magnitude as $|v_\phi - v_{\rm K}|$ one can readily show that the condition for this to hold is that $v_z/c_{\rm s}$ remain $\ll 1$ everywhere within the disc. This can be checked a posteriori for each derived solution of the radially localized model, and we do this for the solutions presented in Paper II. Note that the fulfilment of this condition also implies that the hydrostatic simplification employed in the derivation of the parameter constraints in Sections 4 and 5 should result in a good approximation to the complete numerical solution for the vertical structure of the disc.

3.3 Radial component of the momentum equation

$$\rho v_r\frac{\partial v_r}{\partial r} + \rho v_z\frac{\partial v_r}{\partial z} - \frac{\rho v_\phi^2}{r} + \frac{\partial P}{\partial r} + \rho\frac{\partial\Phi}{\partial r} = \frac{1}{c}(J_\phi B_z - J_z B_\phi). \tag{36}$$

The dominant terms in this equation are the gravitational and centrifugal forces. We can thus simplify it by neglecting the $\partial P/\partial r$ and $\partial v_r/\partial r$ terms. Because of the assumed geometrical thinness, we can also neglect a term of order $(z/r)^2v_{\rm K}^2/r$ in $\partial\Phi/\partial r$. However, to handle the departure from exact Keplerian rotation, we keep the drag force (i.e. the Lorentz force, communicated to the neutrals by ion–neutral collisions; see equation 20) and the $\partial v_r/\partial z$ term. Introducing these changes and using $v_{\rm K}^2 - v_\phi^2 \approx 2v_{\rm K}(v_{\rm K} - v_\phi)$, the radial momentum equation becomes

$$\rho v_z\frac{{\rm d}v_r}{{\rm d}z} + \frac{2\rho v_{\rm K}}{r}(v_{\rm K} - v_\phi) = \frac{1}{c}(J_\phi B_z - J_z B_\phi). \tag{37}$$

3.4 Azimuthal component of the momentum equation

$$\rho v_r\frac{\partial v_\phi}{\partial r} + \frac{\rho v_\phi v_r}{r} + \rho v_z\frac{\partial v_\phi}{\partial z} = \frac{1}{c}(J_z B_r - J_r B_z). \tag{38}$$

In this equation, the torque due to the ion-neutral drag (the right-hand side) and the inward radial transport are important in the

hydrostatic layer, whereas the vertical material transport becomes relevant as the wind region is approached. It is thus appropriate to retain all the terms. Using $v_\phi \approx v_{\rm K}$, we estimate $\partial(r v_\phi)/\partial r \approx v_{\rm K}/2$. With these changes, equation (38) reads

$$\frac{\rho v_r v_{\rm K}}{2r} + \rho v_z \frac{{\rm d}v_\phi}{{\rm d}z} = \frac{1}{c}(J_z B_r - J_r B_z). \tag{39}$$

3.5 Vertical component of the momentum equation

$$\rho v_r \frac{\partial v_z}{\partial r} + \rho v_z \frac{\partial v_z}{\partial z} + \frac{\partial P}{\partial z} + \rho \frac{\partial \Phi}{\partial z} = \frac{1}{c}(J_r B_\phi - J_\phi B_r). \tag{40}$$

The dominant terms in this equation are the thermal pressure gradient and the tidal and magnetic compression terms. This equation can be simplified using

$$\frac{\partial P}{\partial z} = c_{\rm s}^2 \frac{\partial \rho}{\partial z}, \qquad \frac{\partial v_z}{\partial r} \approx 0,$$

$$\rho v_z \frac{\partial v_z}{\partial z} \approx -v_z^2 \frac{\partial \rho}{\partial z}, \qquad \rho \frac{\partial \Phi}{\partial z} \approx \frac{\rho v_{\rm K}^2}{r}\frac{z}{r},$$

where the approximation $\rho v_z = {\rm const}$ was used to obtain the first expression on the second line. The simplified equation is then

$$\left(c_{\rm s}^2 - v_z^2\right)\frac{{\rm d}\rho}{{\rm d}z} + \frac{\rho v_{\rm K}^2}{r}\frac{z}{r} = \frac{1}{c}(J_r B_\phi - J_\phi B_r). \tag{41}$$

3.6 Vertical component of the induction equation

$$\frac{\partial B_z}{\partial t} = -\frac{1}{r}\frac{\partial}{\partial r}(r c E_\phi), \tag{42}$$

where

$$c E_\phi = v_r B_z - v_z B_r + c E'_\phi. \tag{43}$$

In strictly steady-state discs $\nabla \times \boldsymbol{E} = -(1/c)\partial \mathbf{B}/\partial t = 0$, so $\boldsymbol{E}$ can be expressed as a gradient of a scalar function and hence, under the assumption of axisymmetry, $E_\phi = 0$. However, B_z or, equivalently, the poloidal (subscript 'p') magnetic flux function $\Psi(r, z)$ (defined by $2\pi\Psi = \iint \boldsymbol{B}_{\rm p} \cdot {\rm d}\boldsymbol{S}$, where the integral is over a spatially fixed surface that is threaded by the poloidal magnetic field) may still change on the 'long' accretion time-scale $\tau_{\rm a} \equiv r/|v_r|$, corresponding to a radial drift of the poloidal magnetic field through the disc. The mid-plane radial speed of the magnetic flux surface at the radius of interest is given by

$$v_{Br0} = c E_{\phi 0}/B_z \tag{44}$$

(e.g. Nakano, Nishi & Umebayashi 2002). The magnetic flux speed v_{Br0} cannot be fixed arbitrarily (e.g. Ogilvie & Livio 2001) and is, in general, an eigenvalue of the global disc/wind problem. However, in the radially localized formulation of this paper we write $v_{Br0} = -\epsilon_{\rm B} c_{\rm s}$ and treat $\epsilon_{\rm B}$ as a free parameter (see Section 3.13).

3.7 Radial component of the induction equation

$$\begin{aligned}\frac{\partial B_r}{\partial t} &= \frac{\partial}{\partial z}(c E_\phi) \\ &= v_r \frac{\partial B_z}{\partial z} + B_z \frac{\partial v_r}{\partial z} - v_z \frac{\partial B_r}{\partial z} - B_r \frac{\partial v_z}{\partial z} + c \frac{\partial E'_\phi}{\partial z}.\end{aligned} \tag{45}$$

The radial and vertical components of the induction equation can be combined into a single relation by using the poloidal magnetic flux function Ψ defined in Section 3.6. In view of the solenoidal condition on $\boldsymbol{B}$ (equation 22), Ψ satisfies

$$B_z = \frac{1}{r}\frac{\partial \Psi}{\partial r}, \qquad B_r = -\frac{1}{r}\frac{\partial \Psi}{\partial z}.$$

Hence, one can replace equations (42) and (45) by

$$\frac{\partial \Psi}{\partial t} = -r c E_\phi, \tag{46}$$

which implies that, if $\partial B_z/\partial t \neq 0$ (so that $E_\phi \neq 0$) then, strictly, $\partial B_r/\partial t$ need not vanish. We will, however, assume (as was done in WK93) that $\partial B_r/\partial t$ is identically zero. This approximation may be justified on the grounds that a non-zero value of B_r can be established between the mid-plane (where $B_r = 0$) and the top of the disc on the 'short' dynamical time $\tau_{\rm d} \equiv r/v_\phi \approx h/c_{\rm s}$ (where h is again the disc scaleheight) by, for example, the vertical shear in the radial velocity field acting on B_z (consider, respectively, the terms $v_z \partial B_r/\partial z$ and $B_z \partial v_r/\partial z$ in equation 45). Although a fully self-consistent solution in which B_r at the disc surface exactly matches the value determined by the global magnetic field distribution outside the disc (see Section 3.13) may still require a contribution from the slow radial diffusion of the poloidal field, a significant change in the value of B_r at any given radial location can potentially occur on a time much shorter than the accretion time. This situation contrasts with that for the vertical field component B_z (see equations 42 and 43) and is essentially a consequence of the assumed geometrical thinness of the disc. An effectively equivalent approximation was adopted in the Ogilvie & Livio (2001) disc model.

Setting $\partial B_r/\partial t = 0$ in equation (45) implies that E_ϕ is constant with height and hence (using equations 43 and 44) that

$$c E'_\phi = v_z B_r + (v_{Br0} - v_r) B_z \tag{47}$$

at any given radius.

3.8 Azimuthal component of the induction equation

$$\begin{aligned}\frac{\partial B_\phi}{\partial t} &= \frac{\partial}{\partial z}(v_\phi B_z - v_z B_\phi) - \frac{\partial}{\partial r}(v_r B_\phi - v_\phi B_r) \\ &\quad - c\left(\frac{\partial E'_r}{\partial z} - \frac{\partial E'_z}{\partial r}\right).\end{aligned} \tag{48}$$

In analogy with the case of the radial field component discussed in Section 3.7, it can be argued that the explicit-time-derivative term $\partial B_\phi/\partial t$ in equation (48), which describes variations in B_ϕ over the 'long' radial accretion time, can be neglected in comparison with the vertical advection term $v_z \partial B_\phi/\partial z$, which indicates that a measurable azimuthal field component can be established over the 'short' dynamical time, in this case primarily through the radial shear in the azimuthal velocity field acting on B_r (the term $B_r \partial v_\phi/\partial r$ in equation 48). We thus set $\partial B_\phi/\partial t = 0$. In addition, we adopt the following simplifications for the radial-derivative terms:

$$\frac{\partial E'_z}{\partial r} \approx 0, \qquad \frac{\partial (v_r B_\phi)}{\partial r} \approx 0,$$

$$\frac{\partial v_\phi}{\partial r} \approx -\frac{v_{\rm K}}{2r} \Longrightarrow \frac{\partial (v_\phi B_r)}{\partial r} \approx -\frac{3}{2}\frac{B_r v_{\rm K}}{r} - v_\phi \frac{\partial B_z}{\partial z}$$

(see Section 2.1), where we used $\nabla \cdot \boldsymbol{B} = 0$ in the second expression. However, for consistency with the rest of our derivation, we continue

to neglect the vertical variation in B_z. With these approximations, and relating E'_r to E_r through equation (21), we obtain

$$\frac{\mathrm{d}}{\mathrm{d}z}(cE_r) = -\frac{3}{2}\frac{B_r v_\mathrm{K}}{r}. \tag{49}$$

3.9 Ampère's law

The radial and azimuthal components of Ampère's law are, respectively,

$$J_r = -\frac{c}{4\pi}\frac{\mathrm{d}B_\phi}{\mathrm{d}z} \tag{50}$$

and

$$J_\phi = \frac{c}{4\pi}\frac{\mathrm{d}B_r}{\mathrm{d}z}, \tag{51}$$

where we neglected the radial derivative term $(\partial B_z/\partial r)$ in the last expression. The vertical component is

$$J_z = \frac{c}{4\pi r}\left[B_\phi + r\frac{\partial B_\phi}{\partial r}\right] \approx 0. \tag{52}$$

Our neglect of J_z inside the disc is motivated by the fact that, under the thin-disc approximation, the magnitudes of the $\boldsymbol{J}\times\boldsymbol{B}$ terms that include this component will be small in comparison with the terms that involve J_r and J_ϕ.

3.10 Ohm's law

To simplify this equation, we begin by expressing the components of $\boldsymbol{E}'$ parallel and perpendicular to $\boldsymbol{B}$ as

$$\boldsymbol{E}'_\parallel = (\boldsymbol{E}'\cdot\hat{\boldsymbol{B}})\hat{\boldsymbol{B}} = y\boldsymbol{B} \tag{53}$$

and

$$\boldsymbol{E}'_\perp = -\frac{1}{B^2}(\boldsymbol{E}'\times\boldsymbol{B})\times\boldsymbol{B} = -(y\boldsymbol{B}-\boldsymbol{E}'), \tag{54}$$

respectively, where $y \equiv \boldsymbol{E}'\cdot\boldsymbol{B}/B^2$, $B^2 = B_r^2 + B_\phi^2 + B_z^2$. Substituting equations (53) and (54) into equation (24) and using $J_z \approx 0$, we obtain

$$J_r = y(\sigma_\mathrm{O}-\sigma_\mathrm{P})B_r + \frac{\sigma_\mathrm{H}}{B}(E'_z B_\phi - E'_\phi B_z) + \sigma_\mathrm{P}E'_r, \tag{55}$$

$$J_\phi = y(\sigma_\mathrm{O}-\sigma_\mathrm{P})B_\phi + \frac{\sigma_\mathrm{H}}{B}(E'_r B_z - E'_z B_r) + \sigma_\mathrm{P}E'_\phi, \tag{56}$$

$$E'_z = \frac{-B_z(E'_r B_r + E'_\phi B_\phi)(\sigma_\mathrm{O}-\sigma_\mathrm{P})}{B_z^2(\sigma_\mathrm{O}-\sigma_\mathrm{P}) + B^2\sigma_\mathrm{P}} + \frac{\sigma_\mathrm{H}B(E'_r B_\phi - E'_\phi B_r)}{B_z^2(\sigma_\mathrm{O}-\sigma_\mathrm{P}) + B^2\sigma_\mathrm{P}}. \tag{57}$$

3.11 System of ODEs in z

Summarizing, after the simplifications indicated in Section 3.1, we have the following system of non-linear ODEs in z:

$$\rho v_z\frac{\mathrm{d}v_r}{\mathrm{d}z} + \frac{2\rho v_\mathrm{K}}{r}(v_\mathrm{K}-v_\phi) = \frac{1}{c}(J_\phi B_z), \tag{58}$$

$$\rho v_z\frac{\mathrm{d}v_\phi}{\mathrm{d}z} + \frac{\rho v_r v_\mathrm{K}}{2r} = -\frac{1}{c}(J_r B_z), \tag{59}$$

$$\left(c_\mathrm{s}^2 - v_z^2\right)\frac{\mathrm{d}\rho}{\mathrm{d}z} + \frac{\rho v_\mathrm{K}^2}{r}\frac{z}{r} = \frac{1}{c}(J_r B_\phi - J_\phi B_r), \tag{60}$$

$$\frac{\mathrm{d}}{\mathrm{d}z}(cE_r) = -\frac{3}{2}\frac{B_r v_\mathrm{K}}{r}, \tag{61}$$

$$J_r = -\frac{c}{4\pi}\frac{\mathrm{d}B_\phi}{\mathrm{d}z}, \tag{62}$$

$$J_\phi = \frac{c}{4\pi}\frac{\mathrm{d}B_r}{\mathrm{d}z}. \tag{63}$$

3.12 Normalized equations

Equations (58)–(63) form a system of ODEs in v_r, v_ϕ, ρ, E_r, B_ϕ and B_r. The remaining variables – v_z, J_r, J_ϕ, E'_r, E'_ϕ and E'_z – may be found algebraically via equations (21) and (55)–(57), together with the condition $\rho v_z = \mathrm{const}$. Furthermore, as discussed above, under the adopted approximations B_z and E_ϕ are constant with height and $J_z \approx 0$.

These equations can be expressed in dimensionless form by normalizing the variables as follows:

$$\tilde{z} \equiv \frac{z}{h_\mathrm{T}}, \qquad \tilde{\rho} \equiv \frac{\rho(r,z)}{\rho_0(r)}, \tag{64}$$

$$\boldsymbol{w} \equiv \frac{\boldsymbol{v}-v_\mathrm{K}\hat{\boldsymbol{\phi}}}{c_\mathrm{s}}, \ \boldsymbol{w}_\mathrm{E} \equiv \frac{c\boldsymbol{E}/B_0 + v_\mathrm{K}\hat{\boldsymbol{r}}}{c_\mathrm{s}}, \ \boldsymbol{e}' = \frac{c\boldsymbol{E}'}{c_\mathrm{s}B_0}, \tag{65}$$

$$\boldsymbol{j} = \frac{4\pi h_\mathrm{T}\boldsymbol{J}}{cB_0}, \quad \tilde{\boldsymbol{\sigma}} = \frac{4\pi h_\mathrm{T}c_\mathrm{s}\boldsymbol{\sigma}}{c^2}, \quad \boldsymbol{b} \equiv \frac{\boldsymbol{B}}{B_0}, \tag{66}$$

where $h_\mathrm{T} = c_\mathrm{s}r/v_\mathrm{K}$ is the tidal scaleheight of the disc. Note that, under the adopted field symmetry, $B_0 = B_z$ and hence $b_z = 1$. The quantity $\boldsymbol{w}$ represents the normalized (by c_s) fluid velocity in a frame that rotates with the local Keplerian angular velocity $\Omega_\mathrm{K} = v_\mathrm{K}/r$. The quantity $\boldsymbol{w}_\mathrm{E}$ is an analogously reduced effective flux-surface velocity. In particular, note that $w_{\mathrm{E}\phi 0} = v_{Br0}/c_\mathrm{s}$ (see equation 44). One can similarly express the effective mid-plane angular velocity of the magnetic flux surfaces as $\Omega_{\mathrm{B}0} = -cE_{r0}/rB_0$, which implies that $w_{\mathrm{E}r0} = -r(\Omega_{\mathrm{B}0}-\Omega_\mathrm{K})/c_\mathrm{s}$.

With these normalizations, the following dimensionless system of equations is obtained:

$$\frac{\mathrm{d}w_r}{\mathrm{d}\tilde{z}} = \frac{1}{w_z}\left[\frac{a_0^2}{\tilde{\rho}}j_\phi + 2w_\phi\right], \tag{67}$$

$$\frac{\mathrm{d}w_\phi}{\mathrm{d}\tilde{z}} = -\frac{1}{w_z}\left[\frac{a_0^2}{\tilde{\rho}}j_r + \frac{w_r}{2}\right], \tag{68}$$

$$\frac{\mathrm{d}\ln\tilde{\rho}}{\mathrm{d}\tilde{z}} = \frac{1}{1-w_z^2}\left[\frac{a_0^2}{\tilde{\rho}}(j_r b_\phi - j_\phi b_r) - \tilde{z}\right], \tag{69}$$

$$\frac{\mathrm{d}w_{\mathrm{E}r}}{\mathrm{d}\tilde{z}} = -\frac{3}{2}b_r, \tag{70}$$

$$\frac{\mathrm{d}b_r}{\mathrm{d}\tilde{z}} = j_\phi, \tag{71}$$

$$\frac{\mathrm{d}b_\phi}{\mathrm{d}\tilde{z}} = -j_r, \tag{72}$$

$$e'_r = w_{\mathrm{E}r} + w_\phi - w_z b_\phi, \tag{73}$$

$$e'_\phi = -\epsilon_\mathrm{B} + w_z b_r - w_r, \tag{74}$$

$$j_r = y(\tilde{\sigma}_O - \tilde{\sigma}_P)b_r + \frac{\tilde{\sigma}_H}{b}(e'_z b_\phi - e'_\phi) + \tilde{\sigma}_P e'_r, \tag{75}$$

$$j_\phi = y(\tilde{\sigma}_O - \tilde{\sigma}_P)b_\phi + \frac{\tilde{\sigma}_H}{b}(e'_r - e'_z b_r) + \tilde{\sigma}_P e'_\phi, \tag{76}$$

$$e'_z = \frac{-(e'_r b_r + e'_\phi b_\phi)(\tilde{\sigma}_O - \tilde{\sigma}_P)}{(\tilde{\sigma}_O - \tilde{\sigma}_P) + b^2\tilde{\sigma}_P} + \frac{\tilde{\sigma}_H b(e'_r b_\phi - e'_\phi b_r)}{(\tilde{\sigma}_O - \tilde{\sigma}_P) + b^2\tilde{\sigma}_P}. \tag{77}$$

In the above expressions, a_0 is the mid-plane value of $a \equiv v_A/c_s$, where the Alfvén speed is given by

$$v_A = \frac{|\mathbf{B}|}{\sqrt{4\pi\rho}}, \tag{78}$$

and $\epsilon_B \equiv -w_{E\phi} = -v_{Br0}/c_s$ is the normalized value of the vertically uniform E_ϕ.

Note in this connection that w_{Er}, the radial component of the reduced electric field, is expected to be >0 below the base of the wind. This was demonstrated in WK93 for the ambipolar diffusion case and is also true in the Hall and Ohm regimes. The reason for this is that the matter inside the disc rotates at sub-Keplerian speeds because it loses angular momentum to the field, and since the motion of the field lines is controlled by that of the matter (given that the quasi-hydrostatic layer, where the bulk of the mass is located, is thermal pressure-dominated), Ω_B must remain $\lesssim v_\phi/r$. Hence, $w_{Er} = -r(\Omega_B - \Omega_K)/c_s$ would be >0. As the magnetic field bends away from the disc rotation axis ($B_r > 0$ above the mid-plane), Ω_K decreases with distance along the field line, resulting in a corresponding decline in w_{Er}. [Equivalently, equation (70) shows that w_{Er} decreases with $\tilde{z}$ for $b_r > 0$.] Eventually, w_{Er} vanishes at some height above the mid-plane, which roughly coincides with the location of the base of the wind (see Section 4.3).

As the height of the sonic point (denoted by a subscript 's') and the gas density at that location (or, equivalently, the vertical velocity at the mid-plane, given that ρv_z is constant with height) are not known a priori, we treat $\tilde{z}_s$ and w_{z0} as additional variables, which satisfy

$$\frac{d\tilde{z}_s}{d\tilde{z}} = 0 \tag{79}$$

and

$$\frac{dw_{z0}}{d\tilde{z}} = 0. \tag{80}$$

This allows us to find the position of the sonic point and the upward mass flux self-consistently (see Paper II).

3.13 Parameters

The following parameters characterize the disc solutions in our model.

(i) $a_0 \equiv v_{A0}/c_s$, the mid-plane ratio of the Alfvén speed (based on the large-scale vertical field component) to the isothermal sound speed. This parameter measures the strength of the ordered magnetic field that threads the disc.

(ii) $c_s/v_K = h_T/r$, the ratio of the tidal scaleheight to the disc radius. While this parameter, which measures the geometric thinness of the disc, does not appear explicitly in the normalized equations, it nevertheless serves to constrain physically viable solutions (Sections 4 and 5) and is used in matching the disc solutions to the self-similar wind solutions (see Paper II).

(iii) The mid-plane ratios of the conductivity-tensor components: $[\sigma_P/\sigma_\perp]_0$ (or $[\sigma_H/\sigma_\perp]_0$) and $[\sigma_\perp/\sigma_O\ ]_0$. They characterize the conductivity regime of the fluid (Section 2.1). In general, the conductivity-tensor components vary with height, reflecting the ionization structure of the disc (e.g. Salmeron & Wardle 2005). However, the explicit solutions derived in Paper II correspond to a simplified ionization prescription wherein the above ratios remain constant with z.

(iv) The mid-plane Elsasser number $\Lambda_0 \equiv v_{A0}^2/(\Omega_K \eta_{\perp 0})$, where $\eta_\perp \equiv c^2/4\pi\sigma_\perp$ is the 'perpendicular' magnetic diffusivity. This parameter measures the degree of coupling between the neutrals and the magnetic field, with values $\gg 1$ and $\ll 1$ corresponding to strong and weak coupling, respectively.[6]

(v) $\epsilon \equiv -v_{r0}/c_s$, the normalized inward radial speed at the mid-plane. This is a free parameter of the *disc solution*; its value is determined (for given values of the other parameters) at the step where we match it to the BP82 self-similar global wind solution by imposing the Alfvén critical-point constraint on the wind (see Paper II). Although the value of ϵ could in principle be negative (as it, in fact, is in certain viscous disc models; e.g. Takeuchi & Lin 2002), in the context of our model formulation we generally expect $\epsilon > 0$ for physically viable, exclusively wind-driving discs.

(vi) $\epsilon_B \equiv -v_{Br0}/c_s = -cE_{\phi 0}/c_s B_z$, the normalized azimuthal component of the electric field $\boldsymbol{E}$ (vertically constant by equation 45) measures the radial drift speed of the poloidal magnetic field lines. This parameter vanishes in a strictly steady-state solution but is non-zero if the magnetic field lines drift radially on the 'long' accretion time-scale τ_a.

In a global treatment of the disc/wind problem, one can relate ϵ_B to the value of B_r at the disc surface. The latter is determined by the magnetic field distribution outside the disc, and, in the limit of a potential ($\nabla \times \boldsymbol{B} = 0$) external field, can be inferred from the radial distribution of B_z along the disc surface (e.g. Ciolek & Mouschovias 1993; Lubow, Papaloizou & Pringle 1994; Krasnopolsky & Königl 2002). In the numerical solutions presented in Paper II, we simplify the calculation by setting $\epsilon_B = 0$; this condition is then used to determine the value of B_r at the disc surface. WK93, who employed a similar radially localized model, derived solutions for both positive and negative values of ϵ_B (subject to the physically motivated constraint $\epsilon_B < \epsilon$) and showed that disc configurations with the same value of $(\epsilon - \epsilon_B)$ were very similar to each other. This result suggests that setting ϵ_B equal to zero should not strongly impact the generality of the results. Further discussion of this approximation is given in Appendix A.

3.14 Comparison with the multifluid approach

A commonly used alternative to the conductivity-tensor formalism is based on writing down the separate equations of motion for each charged-particle species (e.g. WK93). In this case, instead of employing two independent ratios of the conductivity-tensor components, the fluid can be characterized by the electron and ion Hall

[6] The Elsasser number $\Lambda = v_A^2/(\Omega_K \eta_\perp)$ is distinct from the Lundquist number $S \equiv v_A L/\eta_O$ and from the magnetic Reynolds number $\mathrm{Re_M} \equiv VL/\eta_O$ (where V and L are characteristic speed and length-scale, respectively), which have been used in similar contexts in the literature. This quantity was labelled by the symbol χ in the MRI linear stability analyses of Wardle (1999) and Salmeron & Wardle (2003, 2005), where, in fact, its general form (which allows for variation with height) was considered.

parameters. Indeed, we already noted in Section 2 how the distinct conductivity regimes of the fluid can be delineated directly in terms of β_e and β_i. It is also instructive to evaluate the limiting forms of the magnetic coupling parameter Λ – the 'third parameter' in our classification scheme of viable solutions (see Sections 4 and 5) – in the different conductivity regimes. In the ambipolar diffusion limit $|\beta_e| \gg |\beta_i| \gg 1$ and hence

$$\sigma_\perp \approx \sigma_P \approx \frac{ce}{B}\frac{n_e}{\beta_i} \tag{81}$$

(see equations 13 and 14). In this case Λ reduces to

$$\Upsilon \equiv \frac{\gamma_i \rho_i}{\Omega_K}, \tag{82}$$

the ratio of the Keplerian rotation time to the neutral–ion momentum exchange time. This parameter has emerged as the natural measure of the field–matter coupling in the ambipolar diffusion-dominated disc model of WK93 (where it was labelled η), as well as in studies of the linear (e.g. Blaes & Balbus 1994) and the non-linear (e.g. Mac Low et al. 1995; Brandenburg et al. 1995; Hawley & Stone 1998) evolution of the MRI in such discs. Indeed, since the ions are well coupled to the field in this limit ($|\beta_i| > 1$), the neutrals will be well coupled to the field if their momentum exchange with the charged particles (which is dominated by their interaction with the comparatively massive ions) occurs on a time-scale that is short in comparison with the dynamical time (corresponding to $\Upsilon > 1$).

On the other hand, in the Hall regime $|\beta_e| \gg 1$ and $|\beta_i| \ll 1$, which implies

$$\sigma_\perp \approx |\sigma_H| \approx \frac{cen_e}{|B|} \tag{83}$$

(see equations 12 and 14) and hence $\Lambda = \Upsilon|\beta_i|$. The parameter combination $\Upsilon\,|\beta_i|$, which also figures prominently in linear (e.g. Wardle 1999; Balbus & Terquem 2001) and non-linear (e.g. Sano & Stone 2002a,b) studies of disc MRI in the Hall limit, similarly has a clear physical meaning. Indeed, in contradistinction to the ambipolar diffusion regime, the ions are *not* well coupled to the field in this case ($|\beta_i| < 1$). In order for the neutrals to be well coupled to the field in the Hall regime it is, therefore, not sufficient for them to be well coupled to the ions ($\Upsilon > 1$); rather, the product $\Upsilon\,|\beta_i|$ must be >1 in this case.

Finally, in the Ohm regime, where even the 'electrons' are not well-coupled to the magnetic field ($|\beta_e| \ll 1$),

$$\sigma_\perp \approx \sigma_P \approx \frac{cen_e}{B}\beta_e \tag{84}$$

and therefore $\Lambda = \Upsilon\beta_e\beta_i$, implying a further tightening of the requirement for good coupling between the neutrals and the field.

As we show in Sections 4 and 5, the parameter Υ plays a fundamental role in the theory of wind-driving discs. In fact, it turns out that the condition $\Upsilon \gtrsim 1$ (which, according to the argument given above, signifies good coupling of the neutrals to the field only in the ambipolar diffusion regime) must be satisfied by *all* viable configurations of this type, irrespective of the conductivity domain that characterizes the disc. We elaborate on this point in Section 6.

One can use the definitions of the conductivity components to express their ratios in terms of β_e and β_i. Specializing again to the case $q \ll 1$, we have

$$\frac{\sigma_P}{\sigma_H} = \frac{1+\beta_e\beta_i}{\beta_e}. \tag{85}$$

Furthermore, in the Hall and Ohm limits we get

$$\frac{\sigma_O}{\sigma_H} = \begin{cases} \beta_e & \text{Hall}, \\ \beta_e^{-1} & \text{Ohm}. \end{cases} \tag{86}$$

We also have

$$\tilde{\sigma}_{\perp 0} = \frac{\Lambda_0}{a_0^2}, \tag{87}$$

which follows from the definition of the Elsasser number.

4 PARAMETER CONSTRAINTS

As previously shown by WK93 and Königl (1997), viable wind-driving disc solutions in the strong-coupling regime (defined by Λ_0 not being $\ll 1$) occupy a limited region of parameter space. This region is determined by the requirements that (i) the flow remain sub-Keplerian within the disc, (ii) a wind is driven from the disc surface (i.e. a wind launching criterion is satisfied), (iii) only the upper layers of the disc participate in the outflow and (iv) the rate of heating by the Joule dissipation is bounded by the rate of gravitational energy release. In this section, we generalize these conditions, which were originally derived for discs in the ambipolar diffusion regime, and apply them to discs in the Hall conductivity domain. The corresponding constraints for discs in the Ohm regime are presented in Section 5. The viable solution regions can in general be delineated by the mid-plane values of two independent conductivity-tensor components and of the Elsasser number Λ [see items (*iii*) and (*iv*) in Section 3.13]. While we employ this representation in Paper II, in this paper we use instead the parameters $\psi \equiv \Upsilon_0$, $\beta \equiv 1/\beta_{i0}$ and $q\beta = 1/\beta_{e0}$, which are appropriate to the two-component plasma to which we specialize and afford additional insights into the problem. This choice also allows us to make direct comparisons with the results obtained in WK93 for the ambipolar diffusion regime.

The relevant constraints are derived by focusing, as in WK93, on the quasi-hydrostatic disc region adjacent to the mid-plane, where $w_z^2 \ll 1$. In this limit, the vertical momentum conservation equation (69) reduces to

$$\frac{d\tilde{\rho}}{d\tilde{z}} \approx a_0^2(j_r b_\phi - j_\phi b_r) - \tilde{\rho}\tilde{z}. \tag{88}$$

The last term on the right-hand side of this equation, which represents tidal compression, can generally be neglected in comparison with the magnetic squeezing term (see Section 6). Applying this approximation and substituting for j_ϕ and j_r from equations (71) and (72), respectively, one can then integrate equation (88) to deduce that

$$\tilde{\rho} + \frac{a_0^2}{2}\left(b_r^2 + b_\phi^2\right) \approx \text{const} \tag{89}$$

within the disc and, therefore, that

$$b_{rb}^2 + b_{\phi b}^2 \approx \frac{2}{a_0^2} \tag{90}$$

at the base of the wind (subscript b; the effective surface of the disc), where $\tilde{\rho} \ll 1$. Within the quasi-hydrostatic layer it is appropriate to set $\tilde{\rho} \approx 1$. The two other components of the momentum conservation relation (equations 67 and 68) then reduce to

$$w_\phi \approx -\frac{a_0^2}{2} j_\phi \tag{91}$$

and

$$w_r \approx -2a_0^2 j_r. \tag{92}$$

In the remainder of this section (as well as in Section 5) we assume that the ion mass density $\rho_{\rm i}$ and the collisional coupling coefficient $\gamma_{\rm i}$ (equation 6) are constant with height in the quasi-hydrostatic zone. Under this assumption we can neglect the z-variation of the quantity Υ within this layer and set it equal to $\Upsilon_0 = \psi$.[7]

4.1 Sub-Keplerian flow below the launching region

We seek to identify the regions of parameter space where $w_\phi < 0$ below the launching region, as expected for physically viable solutions (see Section 3.12 and WK93). We begin by expressing j_r and j_ϕ as functions of $b_r, b_\phi, w_{\rm Er}$ and our model parameters by substituting equations (21), (91) and (92) into equation (25). Equation (91) can then be used to deduce the condition that must be satisfied for the flow to remain sub-Keplerian within the disc. The radial and azimuthal components of equation (25) are, respectively,

$$\left[b^2\frac{\sigma_\perp}{\sigma_{\rm O}} + \left(\frac{\sigma_{\rm P}}{\sigma_\perp} - \frac{\sigma_\perp}{\sigma_{\rm O}}\right)(1+b_\phi^2)\right] j_r + \left[b^2\frac{\Lambda_0}{2} + b\frac{\sigma_{\rm H}}{\sigma_\perp} - \left(\frac{\sigma_{\rm P}}{\sigma_\perp} - \frac{\sigma_\perp}{\sigma_{\rm O}}\right) b_r b_\phi\right] j_\phi = b^2\frac{\Lambda_0}{a_0^2} w_{\rm Er} \tag{93}$$

and

$$\left[2b^2\Lambda_0 + b\frac{\sigma_{\rm H}}{\sigma_\perp} + \left(\frac{\sigma_{\rm P}}{\sigma_\perp} - \frac{\sigma_\perp}{\sigma_{\rm O}}\right) b_r b_\phi\right] j_r - \left[b^2\frac{\sigma_\perp}{\sigma_{\rm O}} + \left(\frac{\sigma_{\rm P}}{\sigma_\perp} - \frac{\sigma_\perp}{\sigma_{\rm O}}\right)(1+b_r^2)\right] j_\phi = b^2\frac{\Lambda_0}{a_0^2}\epsilon_{\rm B}. \tag{94}$$

These relations can be cast in terms of $b_r, b_\phi, w_{\rm Er}$ and the parameters ψ, β and q, which are the variables employed by WK93 in their analysis of the ambipolar diffusion regime. Specifically, inverting equations (93) and (94) and substituting

$$b\frac{\sigma_{\rm H}}{\sigma_\perp} = b^2\left(\frac{1-q}{1+q}\right)\frac{\beta\Lambda_0}{\psi}, \tag{95}$$

$$b^2\frac{\sigma_\perp}{\sigma_{\rm O}} = b^2\frac{q\beta^2}{1+q}\frac{\Lambda_0}{\psi} \tag{96}$$

and

$$\left(\frac{\sigma_{\rm P}}{\sigma_\perp} - \frac{\sigma_\perp}{\sigma_{\rm O}}\right) = \frac{b^2}{1+q}\frac{\Lambda_0}{\psi}, \tag{97}$$

we find

$$\begin{pmatrix} j_r \\ j_\phi \end{pmatrix} = \frac{\psi}{a_0^2}\frac{(1+q)}{K}\begin{pmatrix} A_1 & A_2 \\ A_3 & A_4 \end{pmatrix}\begin{pmatrix} w_{\rm Er} \\ \epsilon_{\rm B} \end{pmatrix}. \tag{98}$$

In these expressions

$$A_1 = 1 + q\beta^2 + b_r^2, \tag{99}$$

$$A_2 = \frac{\psi}{2}(1+q) + \beta(1-q) - b_r b_\phi, \tag{100}$$

$$A_3 = 2\psi(1+q) + \beta(1-q) + b_r b_\phi, \tag{101}$$

$$A_4 = -\left(1 + q\beta^2 + b_\phi^2\right) \tag{102}$$

and

$$K = (1+q\beta^2)\left(b_r^2 + b_\phi^2\right) + (1+\beta^2)(1+q^2\beta^2) + \psi(1+q)\left[\frac{5}{2}\beta(1-q) - \frac{3}{2}b_r b_\phi + \psi(1+q)\right]. \tag{103}$$

In the remainder of this paper we assume, for simplicity, that $\epsilon_{\rm B} \approx 0$ (see Section 3.13 and Appendix A). Substituting j_r from equation (92) into equation (98) and using the fact that $w_{\rm Er} > 0$ (see Section 3.12) and $w_r < 0$ below the disc surface, we infer that K must be >0 within the disc. We can also substitute j_ϕ from equation (98) into equation (91) to obtain an explicit expression for the sub-Keplerian flow condition:

$$w_\phi \approx -\frac{\psi(1+q)}{2}\frac{[2\psi(1+q) + \beta(1-q) + b_r b_\phi]w_{\rm Er}}{K} < 0. \tag{104}$$

In the rest of this section and in Section 5 we also specialize to the case $q \ll 1$ (or, equivalently, $1 \pm q \approx 1$), which provides a good approximation for discs in which grains are not the dominant charge carriers. It is straightforward to carry out this analysis in the other case of special interest, namely $q = 1$, which arises when grains dominate both the '+' and the '−' charged components (see Section 6). In the limit $q \ll 1$, the expression for w_ϕ reduces to

$$w_\phi \approx \frac{-\frac{1}{2}\psi(2\psi + \beta + b_r b_\phi)w_{\rm Er}}{(1+q\beta^2)(b_r^2 + b_\phi^2) + (1+\beta^2)(1+q^2\beta^2) + \psi(\frac{5}{2}\beta - \frac{3}{2}b_r b_\phi + \psi)}. \tag{105}$$

In the ambipolar diffusion limit ($|\beta_{\rm e}| \gg |\beta_{\rm i}| \gg 1$) we can take β ($\equiv 1/\beta_{\rm i0}$), $q\beta$ ($\equiv 1/\beta_{\rm e0}$) and $q\beta^2$ ($\equiv 1/\beta_{\rm e0}\beta_{\rm i0}$) to be all $\ll 1$. The right-hand side of equation (105) then reduces to the right-hand side of equation (4.3) in WK93 (where the minus sign in front of the numerator is a typographical error). On the other hand, in the Hall limit ($|\beta_{\rm i}| \ll 1 \ll |\beta_{\rm e}|$) one has $\beta \gg 1$ and $q\beta \ll 1$, but $q\beta^2$ may be either >1 or <1. In the Ohm regime ($|\beta_{\rm i}| \ll |\beta_{\rm e}| \ll 1$) both β and $q\beta$ (and hence also $q\beta^2$) are $\gg 1$.

Given that $w_{\rm Er} > 0$ and $K > 0$ inside the disc, the condition $w_\phi < 0$ implies that

$$\frac{{\rm d}b_r}{{\rm d}b_\phi} = -\frac{j_\phi}{j_r} = -\frac{2\psi + \beta + b_r b_\phi}{1 + q\beta^2 + b_r^2} \tag{106}$$

(where we used equations 98, 99 and 101 in the limit $q \ll 1$) is <0, or

$$-b_r b_\phi < 2\psi + \beta \equiv C \tag{107}$$

below the disc surface. The fact that $b_r b_\phi < 0$ above the mid-plane in turn implies that C must be > 0 and hence that

$$\beta > -2\psi. \tag{108}$$

The form of equation (106) suggests that the Hall parameter regime can be subdivided into four sub-zones, depending on how the ion slip factor $s_0 = 1/q\beta^2$ and the Elsasser number $\Lambda_0 = \psi/|\beta|$ compare with 1 and 1/2, respectively (Königl 1997). In Table 1, where we list the parameter constraints for viable wind-driving disc solutions in the Hall regime, we label these sub-regions by the numerals *i* through *iv*.

Combining equations (90) and (107), we infer that the solutions must satisfy

$$b_{r\rm b}^4 - \frac{2}{a_0^2}b_{r\rm b}^2 + C^2 > 0 \tag{109}$$

[7] In WK93, it was assumed that $\rho_{\rm i}$ and $\gamma_{\rm i}$ are constant from $z = 0$ all the way to the sonic point of the wind, and it was noted that this might be a reasonable approximation to the actual conditions in some protostellar discs on scales $\gtrsim 10^2$ au, where ambipolar diffusion dominates. In the more general case considered in this paper, where we incorporate also the Hall and Ohm diffusivity regimes that are relevant at higher densities, a similar assumption would not be realistic. However, here we only make this approximation in the quasi-hydrostatic layer, where it helps to simplify the analysis.

Table 1. Parameter constraints for wind-driving disc solutions in the limit where the Hall diffusivity dominates. Four distinct cases can be identified, depending on how the values of $s_0 = 1/q\beta^2 = \beta_{e0}\beta_{i0}$ and of $2\Lambda_0 = 2\psi/|\beta| = 2\Upsilon_0|\beta_{i0}|$ compare with 1. The first inequality expresses the requirement that the disc remain sub-Keplerian below the wind zone ($\tilde{z} < \tilde{z}_b$), the second is the wind launching condition (the requirement that the magnetic field lines be sufficiently inclined to the vertical for centrifugal acceleration to occur), the third ensures that the base of the wind is located above the (magnetically reduced) density scaleheight and the fourth specifies that the rate of Joule heating at the mid-plane should not exceed the rate of release of gravitational potential energy there.

Case	Limits		Parameter Constraints – Hall limit (multifluid formulation)								
	$s_0 = \beta_{e0}\beta_{i0}$	$\Lambda_0 = \Upsilon_0\|\beta_{i0}\|$									
i	>1	>1/2	$(2\Upsilon_0)^{-1/2}$	$\lesssim$	a_0	$\lesssim$	2	$\lesssim$	$\epsilon\Upsilon_0$	$\lesssim$	$v_K/2c_s$
ii	>1	<1/2	$\beta_{i0}^{1/2}$	$\lesssim$	a_0	$\lesssim$	$2(\Upsilon_0\beta_{i0})^{1/2}$	$\lesssim$	$\epsilon/2\beta_{i0}$	$\lesssim$	$\Upsilon_0\beta_{i0}\, v_K/c_s$
iii	<1	>1/2	$(2\Upsilon_0)^{-1/2}$	$\lesssim$	a_0	$\lesssim$	2	$\lesssim$	$\epsilon\Upsilon_0\beta_{e0}\beta_{i0}$	$\lesssim$	$v_K/2c_s$
iv	<1	<1/2	$\beta_{i0}^{1/2}$	$\lesssim$	a_0	$\lesssim$	$2(\Upsilon_0\beta_{i0})^{1/2}$	$\lesssim$	$\epsilon\beta_{e0}/2$	$\lesssim$	$\Upsilon_0\beta_{i0}\, v_K/c_s$

in order for the accretion flow to remain sub-Keplerian all the way to the top of the disc. Assuming an equality, we find that solutions only exist if $a_0 > C^{-1/2}$. This translates into $a_0 > (2\psi)^{-1/2}$ for Cases (*i*) and (*ii*) in Table 1 (for which $C \approx 2\psi$) and $a_0 > 1/\beta^{1/2}$ for the remaining two cases (where $C \approx \beta$). These constraints are summarized in the first column of inequalities in the table.[8]

4.2 Wind launching criterion

We identify the wind launching condition using a similar argument to the one developed in WK93. The essence of the argument is that, if no wind were to form, w_z would remain small and equation (88) would be valid throughout the vertical extent of the disc. The right-hand side of this expression is <0 near the mid-plane, but if it became >0 at some height, so that

$$\frac{a_0^2}{\tilde{\rho}}(j_r b_\phi - j_\phi b_r) > \tilde{z}, \tag{110}$$

this would represent an unphysical situation and would lead to a necessary condition for wind launching. We obtain this condition by differentiating both sides of equation (110) with respect to $\tilde{z}$ after substituting for j_ϕ and j_r from equation (98). In the upper layers of the disc the $\tilde{z}$ derivatives of $\tilde{\rho}$, b_r and b_ϕ can be neglected in comparison with the derivative of w_{Er} (given by equation 70). The wind-launching condition then becomes (setting again $\tilde{\rho} \approx 1$)

$$\left[3\psi^2 + \frac{3}{2}\psi\beta - (1+q\beta^2)\right] b_{rb}^2 > (1+\beta^2)(1+q^2\beta^2) + \psi^2 + \frac{5}{2}\beta\psi + (1+q\beta^2)b_{\phi b}^2 + \frac{3}{2}\psi q\beta^2 b_{rb} b_{\phi b}. \tag{111}$$

In the ambipolar diffusion regime, where $\beta, q\beta$ and $q\beta^2$ are $\ll 1$, this expression reduces to equation (4.16) of WK93. That study moreover showed that viable solutions in this regime satisfy $\psi \gtrsim 1$ and $b_{rb} > |b_{\phi b}|$ (see also Section 6), from which it follows that this constraint further reduces to the ideal-MHD wind-launching criterion $b_{rb} > 1/\sqrt{3}$ (BP82) in this case. Using $b_{rb} \approx \sqrt{2}/a_0$ (see equation 90), this condition can be expressed as $a_0 \lesssim \sqrt{6} \approx 2$. The corresponding constraints in the Hall regime are contained in the second column of inequalities in Table 1. Given that the approximation $b_{rb} \approx \sqrt{2}/a_0$ holds in the Hall domain as well (see Section 4.3), it is seen that the ideal-MHD limit of the wind-launching criterion also characterizes Cases (*i*) and (*iii*) in this regime. In the other two Hall sub-regimes (Cases *ii* and *iv*) b_{rb} is required to exceed $(2/\Upsilon_0\beta_{i0})^{1/2}/\sqrt{3}$, which is $>1/\sqrt{3}$ (i.e. the minimum inclination angle of the surface field to the rotation axis that is required for launching a wind is higher than the ideal-MHD value of 30°.).

4.3 Location of the base of the wind

In light of both theoretical and observational arguments (e.g. Königl & Pudritz 2000), only a small fraction of the disc material should participate in the outflow. This condition is implemented by requiring that the base of the wind (which we identify with the height above which the azimuthal velocity becomes super-Keplerian) be located above the magnetically reduced density scaleheight (i.e. $\tilde{z}_b/\tilde{h} > 1$). When this condition is violated, B_ϕ changes sign within the disc, reflecting the attempt by the field to transfer angular momentum to matter before the outflow is initiated (see fig. 6 in WK93 and Paper II).

To formulate this constraint, we begin by estimating the vertical location of the base of the wind. In the hydrostatic approximation, the azimuthal velocity increases to a Keplerian value (i.e. $w_\phi = 0$) when w_{Er} decreases to 0 (see equations 91 and 98). By equation (70), this occurs at

$$\tilde{z}_b \approx \frac{2}{3}\frac{w_{Er0}}{b_{rb}}. \tag{112}$$

Next, we substitute j_{r0} from equation (92) and $w_{r0} = -\epsilon$ into equation (98) to get

$$w_{Er0} = \frac{\epsilon}{2\psi}\,\frac{\psi^2 + (5/2)\psi\beta + (1+\beta^2)(1+q^2\beta^2)}{1+q\beta^2}, \tag{113}$$

where, in the Hall regime ($\beta^2 \gg 1$ and $q^2\beta^2 \ll 1$), the product $(1+\beta^2)(1+q^2\beta^2)$ on the right-hand side reduces to β^2.[9] As an aside, we note that equation (113) can be used to derive a parameter consistency constraint based on the requirement that w_{Er0} (or, equivalently, the mid-plane value of K; see equation 103) must be >0 (see Section 3.12). Indeed, treating this expression as a quadratic equation for β and setting it equal to 0, we find that viable solutions in the Hall regime require $\beta < -2\ \psi$ or $\beta > -\psi/2$. In view of equation (108), it follows that

$$\beta > -\psi/2 \qquad \text{in the Hall regime.} \tag{114}$$

In the wind-driving discs that are of interest to us the density scaleheight ($\tilde{h}$) is generally reduced by magnetic squeezing

[8] Note that, although the ion Hall parameter can in principle assume a negative value, all entries of $\beta_{i0}^{1/2}$ in Tables 1 and 3 in fact correspond to $\beta_{i0} > 0$ (see Section 6).

[9] A more general expression for w_{Er0}, in which no restriction is placed on the value of q, is given by equation (A11) in WK93.

Table 2. Key properties of viable disc solutions in the Hall regime. Listed, in order, are the mid-plane values of $|\mathrm{d}b_r/\mathrm{d}b_\phi|$, the magnetically compressed scaleheight in units of the tidal scaleheight ($\tilde{h} \equiv h/h_\mathrm{T}$), the similarly normalized vertical location of the base of the wind $\tilde{z}_\mathrm{b}$ in units of $\tilde{h}$ and the normalized Joule dissipation rate $\boldsymbol{j}\cdot\boldsymbol{e}'$ at the mid-plane.

Case	Limits		Solution characteristics – Hall limit			
	$s_0 = \beta_{\mathrm{e}0}\beta_{\mathrm{i}0}$	$\Lambda_0 = \Upsilon_0\lvert\beta_{\mathrm{i}0}\rvert$	$\lvert\mathrm{d}b_r/\mathrm{d}b_\phi\rvert_0$	$\tilde{h}$	$\tilde{z}_\mathrm{b}/\tilde{h}$	$(\boldsymbol{j}\cdot\boldsymbol{e}')_0$
i	>1	>1/2	$2\Upsilon_0$ (>1)	$a_0/\epsilon\Upsilon_0$	$(\epsilon\Upsilon_0)^2/3\sqrt{2}$	$\epsilon^2\Upsilon_0/a_0^2$
ii	>1	<1/2	$1/\beta_{\mathrm{i}0}$ (>1)	$2\,a_0\beta_{\mathrm{i}0}/\epsilon$	$\epsilon^2/6\sqrt{2}\Upsilon_0\beta_{\mathrm{i}0}^3$	$\epsilon^2/4\Upsilon_0\beta_{\mathrm{i}0}^2\,a_0^2$
iii	<1	>1/2	$2\Upsilon_0\,\beta_{\mathrm{e}0}\beta_{\mathrm{i}0}$ (>1)	$a_0/\epsilon\Upsilon_0\beta_{\mathrm{i}0}\beta_{\mathrm{e}0}$	$(\epsilon\Upsilon_0\beta_{\mathrm{e}0}\beta_{\mathrm{i}0})^2/3\sqrt{2}$	$\epsilon^2\Upsilon_0\beta_{\mathrm{e}0}\beta_{\mathrm{i}0}/a_0^2$
iv	<1	<1/2	$\beta_{\mathrm{e}0}$ (>1)	$2a_0/\epsilon\,\beta_{\mathrm{e}0}$	$(\epsilon\beta_{\mathrm{e}0})^2/6\sqrt{2}\Upsilon_0\beta_{\mathrm{i}0}$	$\epsilon^2\beta_{\mathrm{e}0}/4\Upsilon_0\beta_{\mathrm{i}0}a_0^2$

($\tilde{h} \equiv h/h_\mathrm{T} < 1$; see Section 6 and WK93). To obtain an expression for $\tilde{h}$ we first approximate the surface values of b_r and b_ϕ by $b_{r\mathrm{b}} \approx \tilde{z}_\mathrm{b}(\mathrm{d}b_r/\mathrm{d}\tilde{z})_0$ and $b_{\phi\mathrm{b}} \approx \tilde{z}_\mathrm{b}(\mathrm{d}b_\phi/\mathrm{d}\tilde{z})_0$, respectively.[10] Then, using equation (106), we deduce

$$\left|\frac{b_{r\mathrm{b}}}{b_{\phi\mathrm{b}}}\right| \approx \left|\frac{\mathrm{d}b_r}{\mathrm{d}b_\phi}\right|_0 = \frac{2\psi+\beta}{1+q\beta^2}, \tag{115}$$

which is readily verified to be >1 in all the Hall sub-regimes. These results are presented in column 4 of Table 2, which summarizes the key properties of our wind solutions for the various Hall sub-regimes considered in this section. Neglecting the b_ϕ term in equation (88) and approximating $\tilde{\rho} \approx 1$ and $b_r \approx \tilde{z}(\mathrm{d}b_r/\mathrm{d}\tilde{z})_0$, we find

$$\frac{\mathrm{d}\tilde{\rho}}{\mathrm{d}\tilde{z}} \approx -\left[a_0^2\left(\frac{\mathrm{d}b_r}{\mathrm{d}\tilde{z}}\right)_0^2 + 1\right]\tilde{z}. \tag{116}$$

As we show in Section 6, magnetic compression (represented by the first term on the right-hand side of equation 116) dominates tidal squeezing (the second term on the right-hand side) in all viable wind-driving disc solutions. Defining the scaleheight $\tilde{h}$ by relating it to an effective Gaussian density distribution, so that

$$\frac{\mathrm{d}\tilde{\rho}}{\mathrm{d}\tilde{z}} = -\frac{\tilde{z}}{\tilde{h}^2}, \tag{117}$$

we thus infer

$$\tilde{h} \approx \frac{1}{a_0}\left(\frac{\mathrm{d}b_r}{\mathrm{d}\tilde{z}}\right)_0^{-1}. \tag{118}$$

By substituting for $(\mathrm{d}b_r/\mathrm{d}\tilde{z})_0$ in equation (118) from equations (71) and (98), we can express $\tilde{h}$ in terms of the disc parameters as

$$\tilde{h} \approx \frac{2a_0}{\epsilon}\,\frac{1+q\beta^2}{2\psi+\beta}. \tag{119}$$

Similarly, combining equations (90), (112), (113) and (119), we get the desired expression for the location of the base of the wind in the Hall regime:

$$\frac{\tilde{z}_\mathrm{b}}{\tilde{h}} \approx \frac{\epsilon^2(2\psi+\beta)}{6\sqrt{2}\psi}\,\frac{\psi^2+(5/2)\psi\beta+\beta^2}{(1+q\beta^2)^2}. \tag{120}$$

Expressions for $\tilde{h}$ valid for Cases (*i*)–(*iv*) are listed in column 5 of Table 2. Equation (120), which is listed in column 6 of that table, can be used to express the constraint $\tilde{z}_\mathrm{b}/\tilde{h} > 1$ in each of the four Hall sub-regimes. This constraint is shown in the third column of inequalities in Table 1.

[10] We will not use these expressions to estimate the actual magnitudes of the transverse magnetic field components at the base of the wind (rather than just their ratio) both because the assumption of a linear scaling of the field components with $\tilde{z}$ is not expected to remain accurate above a density scaleheight and because of the approximation involved in the definition (112) of $\tilde{z}_\mathrm{b}$; instead, we will use equation (90) for this purpose.

4.4 Dissipation rate

This constraint, represented by the last set of inequalities in Table 1, limits the rate of heating by Joule dissipation at the mid-plane to less than the rate of gravitational potential energy release at that location (Königl 1997),

$$(\boldsymbol{j}\cdot\boldsymbol{e}')_0 < \frac{\epsilon}{2a_0^2}\frac{v_\mathrm{K}}{c_\mathrm{s}}, \tag{121}$$

where, by equations (26), (27) and (52),

$$\begin{aligned}(\boldsymbol{j}\cdot\boldsymbol{e}')_0 &= \frac{a_0^2}{\psi}(1+q\beta^2)(j_{r0}^2+j_{\phi0}^2)\\ &= \frac{\epsilon^2}{4\psi a_0^2}(1+q\beta^2)\left[1+\left(\frac{2\psi+\beta}{1+q\beta^2}\right)^2\right].\end{aligned} \tag{122}$$

The expression (122) is shown in column 7 of Table 2 for each of the Hall sub-regimes.

5 THE OHM REGIME

In this section, we consider the parameter constraints on viable wind-driving disc solutions for discs in the Ohm diffusivity regime. The corresponding constraints for discs in the Hall regime were derived in Section 4 using the hydrostatic approximation, and here we either directly apply the results presented in that section or else further generalize them to cover also the Ohm domain. We again adopt the multifluid formalism in a weakly ionized 'ion'–'electron' gas with $q \ll 1$, in which the Ohm regime is defined by the inequalities $|\beta_{\mathrm{i}0}| \ll |\beta_{\mathrm{e}0}| \ll 1$ (or, equivalently, $|\beta| \gg q|\beta| \gg 1$). We also continue to assume that $\epsilon_\mathrm{B} \approx 0$.

5.1 Sub-Keplerian flow below the launching region

All the results derived in Section 4.1 are applicable in this regime. In particular, a necessary condition for a solution to exist is that the inequality $a_0 > C^{-1/2}$ is satisfied, where C, given by equation (107), is equal to 2ψ (where $\psi = \Upsilon_0$) or to β in the limits where $\psi/|\beta|$ is $\gg 1/2$ or $\ll 1/2$, respectively. The magnitude of this parameter combination thus provides a natural classification criterion, similarly to the situation in the Hall regime. However, in contrast with the Hall case, in which the factor $q\beta^2$ in the denominator of equation (106) can be either >1 or <1, in the Ohm limit $q\beta^2 \gg 1$ and this parameter combination cannot be used to identify the relevant parameter sub-regimes. A suitable combination can nevertheless be found by using the relation (106) to determine which transverse magnetic field component (radial or azimuthal) dominates at the disc surface (see equation 115). In the limit $|\beta| \gg 2\psi$ we have $|b_{r\mathrm{b}}/b_{\phi\mathrm{b}}| \approx 1/q\beta \ll 1$, but in the opposite limit ($2\psi \gg |\beta|$) this ratio is given by $|b_{r\mathrm{b}}/b_{\phi\mathrm{b}}| \approx 2\psi/q\beta^2$, which can be either >1 or <1.

This suggests that the parameter combination $\psi/q\beta^2$ could serve to sub-divide the parameter regime $\psi/\beta > 1/2$. As we verify in the subsequent sections, this is indeed a proper choice. This result is not surprising given the fact that, in the Ohm regime, $\psi/q\beta^2$ is equal to the Elsasser number Λ_0 (defined in Section 3.13) and that Λ_0 plays a similar role in the Hall regime (where it is equal to $\psi/|\beta|$).

5.2 Wind launching criterion

In analyzing the inequality given by equation (111) in the Ohm limit, we consider separately the cases $\psi/|\beta| > 1/2$ and $\psi/|\beta| < 1/2$. As we noted in Section 5.1, the first case can be sub-divided according to whether Λ_0 is $>1/2$ or $<1/2$. When $\Lambda_0 > 1/2$, the dominant terms on both the left-hand side and the right-hand side of equation (111) are the ones containing the factor ψ^2, and we recover the BP82 launching condition of a centrifugally driven, ideal-MHD wind from a Keplerian disc, $b_{r\rm b} > 1/\sqrt{3}$. However, the application of the above equation to the second sub-regime, in which the inequalities $|\beta| < 2\psi < q\beta^2$ are satisfied, is less straightforward. Indeed, while one can readily verify that the term involving ψ^2 again dominates the left-hand side of equation (111) in this case, on the right-hand side of this equation either the first term or the last term could potentially dominate. Assuming that the first term ($\sim q^2\beta^4$) in fact dominates, one can substitute $b_{r\rm b}^2 \approx (2/a_0^2)(2\psi/q\beta^2)^2$ from equations (90) and (115) into equation (111) to infer that the factor $6\psi^2/a_0^2q^2\beta^4$ is $>(q\beta^2/2\psi)^2 > 1$. But in the chosen parameter regime this factor is equal to the ratio of the absolute magnitude of the last term on the right-hand side of equation (111) to the first term on the right-hand side of this equation, which is a contradiction (as we assumed that the first term on the right-hand side dominates). A self-consistent solution can thus be obtained only if the ratio of the absolute values of the last and first terms on the right-hand side of equation (111) is required from the start to exceed 1, in which case the inequality expressed by this equation would be trivially satisfied (with the left-hand side being >0 and the right-hand side – which is proportional to $b_{r\rm b}b_{\phi\rm b}$ – being <0). This requirement, in turn, provides an effective wind-launching condition on the inclination of surface poloidal field: $b_{r\rm b} > 2/\sqrt{3}$.[11]

Turning now to the case $\psi/|\beta| < 1/2$, we find that it is again possible to choose between two alternatives: either $\psi > q|\beta|$ or $\psi < q|\beta|$. The first alternative is similar to the just-discussed $\psi/|\beta| > 1/2$, $\Lambda_0 < 1/2$ sub-regime in that one can immediately identify the dominant term on the left-hand side of equation (111) (which in this instance involves the factor $3\psi\beta/2$) even as the choice between the first and last terms on the right-hand side of this equation appears to be unclear. The assumption that the first term on the right-hand side dominates again leads to a contradiction, so in this case, too, one is led to impose the requirement that the last term always dominates the first term on the right-hand side of equation (111). This requirement, in turn, again implies an effective wind-launching criterion, which in this case is $b_{r\rm b} > [(4/3)(\beta/2\psi)]^{1/2} (> 2/\sqrt{3})$.[12] The second alternative, corresponding to the parameter regime $q|\beta| < \psi < |\beta|/2$, does not allow the launching condition to be satisfied since it implies that, while the right-hand side of equation (111) remains >0, the left-hand side is dominated by the last term and is therefore <0. We therefore exclude this parameter regime from further consideration in the ensuing sections, in which we continue to verify that the three other Ohm sub-regimes that we have identified are compatible with wind-driving disc solutions that obey all the relevant physical requirements.

[11] This condition implies a minimum inclination angle of the surface poloidal field to the rotation axis of $\simeq 49^\circ$, as compared with 30° for the ideal MHD-like case ($b_{r\rm b} > 1/\sqrt{3}$).

[12] We have implicitly assumed that the Hall parameters are >0 in this case; this is explicitly justified in Section 6.

5.3 Location of the base of the wind

In the Hall regime, we deduced that all viable solutions satisfy $|b_{r\rm b}/b_{\phi\rm b}| \approx |{\rm d}b_r/{\rm d}b_\phi|_0 \gg 1$, and we used this approximation in deriving the expressions (118) and (120) for the normalized density scaleheight $\tilde{h}$ and discheight $\tilde{z}_{\rm b}$. However, as already noted in Section 5.1, in the Ohm case this inequality could in principle be reversed, in which case the above expressions would need to be modified. This can be done through a straightforward generalization of the derivations presented in Section 4.3. Using equation (115) and defining

$$D(\psi,\beta) \equiv \left(\frac{{\rm d}b_r}{{\rm d}b_\phi}\right)_0^2 = \left(\frac{2\psi+\beta}{1+q\beta^2}\right)^2, \tag{123}$$

we obtain

$$\tilde{h} = \frac{2a_0}{\epsilon}[1+D(\psi,\beta)]^{-1/2}, \tag{124}$$

$$b_{r\rm b} \approx \frac{\sqrt{2}}{a_0}[1+1/D(\psi,\beta)]^{-1/2} \tag{125}$$

and

$$\frac{\tilde{z}_{\rm b}}{\tilde{h}} \approx \frac{\epsilon^2}{6\sqrt{2}\psi}\frac{\psi^2+(5/2)\psi\beta+(1+\beta^2)(1+q^2\beta^2)}{2\psi+\beta}[1+D(\psi,\beta)]. \tag{126}$$

It can be readily verified that in the Hall limit these results reduce to the corresponding expressions presented in Section 4.3.

5.4 Dissipation rate

The results of Section 4.4, given by equations (121) and (122), continue to apply also in the Ohm regime. Note that the second of the above equations can be written in the form

$$(\boldsymbol{j}\cdot\boldsymbol{e}')_0 = \frac{\epsilon^2}{4\psi a_0^2}(1+q\beta^2)\,[1+D(\psi,\beta)]\,. \tag{127}$$

5.5 Results

The results of the foregoing analysis are collected in Tables 3 and 4, which are patterned on Tables 1 and 2, respectively, in Section 4 (where the corresponding data for the Hall regime are presented). The implications of these results are discussed in conjunction with those of our findings for the Hall and ambipolar-diffusion regimes in Section 6.

5.6 Formulation in terms of scalar conductivity

As we noted in Section 2.1, the analysis of the problem in the Ohm regime can be alternatively carried out in terms of the scalar conductivity $\sigma_{\rm O}$ (equation 11). In the case of a two-component plasma with $q \ll 1$ this is just the 'electron' electrical conductivity $\sigma_{\rm e}$ (equation 27). With our adopted normalization (see equation 66),

Table 3. Parameter constraints for wind-driving disc solutions in the limit where the Ohm diffusivity dominates. Three distinct cases can be identified, as indicated. The meaning of the four inequalities in each sub-regime is the same as in Table 1. The parameters ψ, β and $q\beta$ used in the text are related to the parameters employed in the table through $\psi = \Upsilon_0$, $\beta = 1/\beta_{i0}$ and $q\beta = 1/\beta_{e0}$.

Case	Limits		Parameter constraints – Ohm limit (multifluid formulation)								
	$\Upsilon_0\lvert\beta_{i0}\rvert$	$\Lambda_0 = \Upsilon_0\lvert\beta_{e0}\rvert\,\lvert\beta_{i0}\rvert$									
i	$>1/2$	$>1/2$	$(2\Upsilon_0)^{-1/2}$	$\lesssim$	a_0	$\lesssim$	2	$\lesssim$	$\epsilon\Upsilon_0\beta_{e0}\beta_{i0}$	$\lesssim$	$v_K/2c_s$
ii	$>1/2$	$<1/2$	$(2\Upsilon_0)^{-1/2}$	$\lesssim$	a_0	$\lesssim$	$2\Upsilon_0\beta_{e0}\beta_{i0}$	$\lesssim$	$\epsilon/2$	$\lesssim$	$\Upsilon_0\beta_{e0}\beta_{i0}v_K/c_s$
iii	$<1/2$	$>\lvert\beta_{i0}\rvert$	$\beta_{i0}^{1/2}$	$\lesssim$	a_0	$\lesssim$	$2(\Upsilon_0\beta_{i0})^{1/2}\beta_{e0}$	$\lesssim$	$\epsilon/2$	$\lesssim$	$\Upsilon_0\beta_{e0}\beta_{i0}\ v_K/c_s$

Table 4. Key properties of viable disc solutions in the Ohm regime. See the caption to Table 2 for a description of the listed quantities.

Case	Limits		Solution characteristics – Ohm limit				
	$\Upsilon_0\lvert\beta_{i0}\rvert$	$\Lambda_0 = \Upsilon_0\lvert\beta_{e0}\rvert\,\lvert\beta_{i0}\rvert$	$\lvert db_r/db_\phi\rvert_0$		$\tilde{h}$	$\tilde{z}_b/\tilde{h}$	$(\boldsymbol{j}\cdot\boldsymbol{e}')_0$
i	$>1/2$	$>1/2$	$2\Upsilon_0\beta_{e0}\beta_{i0}$	(>1)	$a_0/\epsilon\Upsilon_0\beta_{e0}\beta_{i0}$	$(\epsilon\Upsilon_0)^2/3\sqrt{2}$	$\epsilon^2\Upsilon_0\beta_{e0}\beta_{i0}/a_0^2$
ii	$>1/2$	$<1/2$	$2\Upsilon_0\beta_{e0}\beta_{i0}$	(<1)	$2a_0/\epsilon$	$(\epsilon/\Upsilon_0\beta_{e0}\beta_{i0})^2/12\sqrt{2}$	$\epsilon^2/4\Upsilon_0\beta_{e0}\beta_{i0}a_0^2$
iii	$<1/2$	$>\lvert\beta_{i0}\rvert$	β_{e0}	(>1)	$2\,a_0/\epsilon$	$(\epsilon/\beta_{e0})^2/6\sqrt{2}\Upsilon_0\beta_{i0}$	$\epsilon^2/4\Upsilon_0\beta_{e0}\beta_{i0}a_0^2$

the corresponding dimensionless conductivity at the mid-plane of the disc is

$$\tilde{\sigma}_{e0} = \frac{4\pi h_T c_s \sigma_e}{c^2} = \frac{h_T c_s}{\eta_{O0}} = \frac{\Upsilon_0\beta_{e0}\beta_{i0}}{a_0^2}. \tag{128}$$

From equation (128) it is seen that, in the Ohm regime, $\Lambda_0 = a_0^2\tilde{\sigma}_e$.[13] This makes it possible to relate the results derived in this section to the equivalent scalar-conductivity formulation. In particular, Cases (*i*) and (*ii*) identified above correspond to $a_0^2\tilde{\sigma}_e$ being $>1/2$ and $<1/2$, respectively. Resistive-MHD disc models that have appeared in the literature typically use Ohm's law in the form $\boldsymbol{E} = -\boldsymbol{v}\times\boldsymbol{B}/c + \boldsymbol{J}/\sigma_e$ and ignore the second (Hall) term on the right-hand side of the more general expression given by equation (25). On the face of it, this might be justified by the fact that the ratio of the conductivity prefactors of the second and first terms on the right-hand side of this equation, $\lvert\sigma_H\rvert\,\sigma_O/\sigma_\perp^2$, is $\sim\lvert\beta_e\rvert$, which is $\ll 1$ in the Ohm regime. However, this argument does not account for the fact that the Hall term in the expression for $\boldsymbol{E}'$ is perpendicular to $\boldsymbol{J}$, which implies, in particular, that the Hall term appears in the prefactor of the *radial* current density J_r in the normalized expression for the *azimuthal* electric field component E_ϕ (equation 94). The only other contributor to this prefactor at $z = 0$ is associated with the advective ($\propto \boldsymbol{v}\times\boldsymbol{B}/c$) term, which could in principle be subordinate to the Hall-current term. Now, these two terms (Hall and advective) in equation (94) correspond to the two terms (β and 2ψ, respectively) in the numerator of the expression for $\lvert db_r/db_\phi\rvert_0$ (equation 115) that are used in our solution classification scheme for the Ohm regime. In Cases (*i*) and (*ii*) $\Upsilon_0\lvert\beta_{i0}\rvert = a_0^2\tilde{\sigma}_{e0}/\lvert\beta_{e0}\rvert > 1/2$ and so the Hall term can be neglected, but in Case (*iii*) this inequality is reversed and the Hall term dominates.

6 DISCUSSION

The first term within the first pair of parentheses on the right-hand side of equation (122) represents the ohmic contribution to the Joule dissipation in the disc, whereas the second term corresponds to the ambipolar dissipation. (The Hall term in Ohm's law, i.e. the term $\propto \boldsymbol{J}\times\boldsymbol{B}$ in equations 25 and 26, does not contribute to the $\boldsymbol{J}\cdot\boldsymbol{E}'$ dissipation.) This suggests (see Königl 1997) that the slip factor $s_0 = 1/q\beta^2 = \beta_{e0}\beta_{i0}$ can be used to distinguish between ambipolar diffusion-like ($\beta_{e0}\beta_{i0} > 1$) and Ohm-like ($\beta_{e0}\,\beta_{i0} < 1$) sub-regimes in the nominal Hall parameter domain ($\lvert\beta_{i0}\rvert < 1 < \lvert\beta_{e0}\rvert$).[14] For comparison, both $\beta_{e0}\beta_{i0} > 1$ *and* $\lvert\beta_{i0}\rvert > 1$ must hold in the actual ambipolar diffusion regime, whereas both $\beta_{e0}\,\beta_{i0} < 1$ *and* $\lvert\beta_{e0}\rvert < 1$ must be satisfied in the genuine Ohm regime. This criterion forms the basis of the classification given in the second column of Table 1. The relevance of this criterion is demonstrated by the fact that the first row of inequalities (Case *i*) exactly reproduces the corresponding constraints in the ambipolar diffusion case (see WK93 and Königl 1997) and that the third row (Case *iii*) is identical to the first row of inequalities in Table 3 (Case *i* in the Ohm regime).[15]

The third column in Table 1 classifies the solutions according to the value of the magnetic coupling parameter Λ_0 (the Elsasser number, which in the Hall regime is equal to $\Upsilon_0\lvert\beta_{i0}\rvert$). Although the constraints obtained for large ($\Lambda_0 > 1/2$; Cases *i* and *iii*) and small ($\Lambda_0 < 1/2$; Cases *ii* and *iv*) values of Λ_0 are clearly distinct in their forms, it is interesting to note that the sub-Keplerian rotation and wind-launching requirements (the first and second inequalities, respectively) together imply that $\Upsilon_0 \gtrsim 1$ *in all cases*. This inequality already follows directly from the conditions $\Upsilon_0\lvert\beta_{i0}\rvert > 1/2$ and $\lvert\beta_{i0}\rvert < 1$ that define the Hall Cases (*i*) and (*iii*), but it is noteworthy that all viable solutions in the Hall domain satisfy this constraint, which was previously inferred in the ambipolar diffusion regime (see WK93). This result can be visualized by plotting the sub-Keplerian-rotation and wind-launching constraints for each of the Hall sub-regimes. First, however, we present the relevant curves in the ambipolar diffusion limit (Fig. 1; cf. fig. 3 in WK93). The dark, solid lines in this figure show the run of b_r versus b_ϕ, computed from equation (106), for $\Upsilon_0 = 10, 2$ and 1. In fully sub-Keplerian discs db_r/db_ϕ must be <0 below the base of the wind (i.e. for $\tilde{z} < \tilde{z}_b$; see equations 105 and 106). This condition constrains viable solutions to lie *to the left* of the long-dashed curve that marks the locus of points where $db_r/db_\phi = 0$. On the other hand, these solutions must also satisfy the wind-launching criterion (equation 111), which constrains them to reside *above* the light solid line for the given

[13] This also follows directly from the relation (87) in this limit.

[14] This can also be seen directly from equation (34), which implies that $s = \eta_A/\eta_O$.

[15] These correspondences apply also to the solution characteristics listed in Tables 2 and 4.

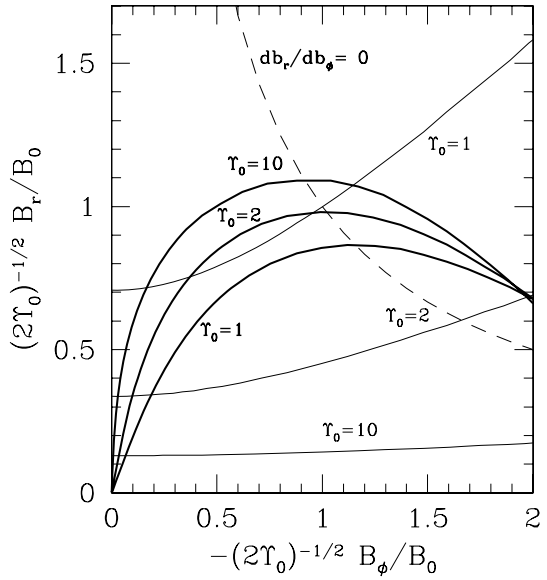

Figure 1. Plots of b_r versus b_ϕ [each normalized by $(2\Upsilon_0)^{1/2}$] in the quasi-hydrostatic region of the disc (dark solid lines) for $\Upsilon_0 = 1, 2$ and 10 in the limit where ambipolar diffusion dominates. Physically viable solutions must satisfy two constraints. First, they must lie to the left of the long-dashed line, which marks the point where d b_r/d b_ϕ changes sign: this ensures that the azimuthal velocity is sub-Keplerian within the disc (i.e. w_ϕ, given by equation 105, is <0 for $\tilde{z} < \tilde{z}_b$). Secondly, they must also lie above the light solid line for the corresponding value of Υ_0, so that the wind-launching criterion (equation 111) is satisfied. It is evident from the figure that these two constraints together imply $\Upsilon_0 \gtrsim 1$.

value of Υ_0. It is evident from these plots that no physically viable solutions exist for $\Upsilon_0 < 1$. The corresponding curves for Cases (*i*)–(*iv*) in the Hall limit are shown in the four panels of Fig. 2: they confirm that viable solutions satisfy $\Upsilon_0 \gtrsim 1$ also in all the Hall sub-regimes.

As was shown in Section 5, the magnitude of the parameter combination $\Upsilon_0|\beta_{i0}|$ compared to 1/2 is one of the classification criteria also in the Ohm regime (see the second column in Table 3). When $\Upsilon_0|\beta_{i0}| > 1/2$ the second classification criterion in the Ohm regime can again be expressed in terms of the Elsasser number Λ_0 (which in this limit equals $\Upsilon_0\, \beta_{e0}\beta_{i0}$) being either >1/2 (the Ohm Case *i*) or <1/2 (the Ohm Case *ii*; see the third column in Table 3). Similarly to the situation in the Hall Cases (*i*) and (*iii*), the fact that $|\beta_{i0}| < 1$ implies that Υ_0 must be $\gtrsim$1 also in these two Ohm sub-regimes. The third Ohm sub-regime is defined by $\Upsilon_0|\beta_{i0}| < 1/2$ and $\Upsilon_0|\beta_{e0}| > 1$. Since $|\beta_{e0}| < 1$ in the Ohm domain, it follows that $\Upsilon_0 \gtrsim 1$ in this case too.

The parameter Υ_0 (which is equal to Λ_0 in the ambipolar diffusion regime) thus turns out to be of fundamental importance in the theory of diffusive wind-driving discs in that it is inferred to be $\gtrsim$1 for all viable solutions irrespective of the conductivity regime. Physically, the condition $\Upsilon_0 \gtrsim 1$ expresses the requirement that the momentum exchange time of the neutrals with the particles that dominate the momentum of the charged species (the comparatively massive 'ions' in our formulation) be shorter than the dynamical time (i.e. the Keplerian orbital time). This requirement is evidently more basic than having the nominal neutral–field coupling parameter Λ_0 be $\gtrsim$1. In fact, as noted above, some of the distinct parameter sub-regimes that we identified are defined by the inequality $\Lambda_0 < 1/2$. However, even in the latter cases Λ_0 remains bounded from below by a numerical factor that typically is not $\ll$1 ($\Lambda_0 \gtrsim a_0^2/3$ and $\Lambda_0 \gtrsim a_0/\sqrt{6}$ in the Hall and Ohm regimes, respectively, from the wind launching condition; see Tables 1 and 3).

The lower bounds on Λ_0 reflect our assumption that the modelled discs are strongly coupled, which implies, in particular, that the transverse magnetic field component starts to grow already at $\tilde{z} = 0$ (see the solution curves presented in Paper II). As was first demonstrated by Li (1996) and Wardle (1997), viable solutions of discs in which the bulk of the matter is not well coupled to the field can also be constructed.[16] In these solutions, significant field-line bending that enables a centrifugally driven wind to be launched from the disc surface only starts well above the mid-plane. Although the basic disc properties above the height where b_r starts to increase rapidly are similar to those of strongly coupled configurations, this location depends on the detailed density and ionization structure of the disc and cannot be readily determined a priori. It roughly coincides with the height where $|\mathrm{d}b_r/\mathrm{d}b_\phi|$ (estimated using equation 115), which is typically $\ll 1$ at the mid-plane under these circumstances, has grown to a value $\sim$1. However, disc material already moves inward below this height on account of the fact that $|b_\phi|$ becomes $\lesssim 1$ when b_r is still $\ll$1, which means that a significant magnetic torque (of density $\propto B_z \mathrm{d}B_\phi/\mathrm{d}z$) can be exerted even at lower elevations.

The magnitude of the field-strength parameter a_0 is bounded from below by the sub-Keplerian rotation constraint (the first inequality in Tables 1 and 3) and from above by the wind-launching constraint (the second inequality in Tables 1 and 3). If the magnetic field is too weak it will not drive an outflow but instead mediate a 'two-channel' flow within the disc (see Salmeron et al. 2007). On the other hand, if the field is too strong it will not bend out sufficiently to drive a centrifugal wind. Our typical solutions are characterized by $a_0 \lesssim 1$. We have found that the ratio $|b_{r\mathrm{b}}/b_{\phi\mathrm{b}}|$ of the radial to azimuthal magnetic field amplitudes at the disc surface is >1 in the ambipolar diffusion regime (WK93) as well as in all the Hall sub-regimes (Section 4.3). However, in the Ohm regime this is true only for Case (*i*), whereas in the other two Ohm sub-regimes $|b_{\phi\mathrm{b}}| > b_{r\mathrm{b}}$ (see Table 4). Nevertheless, even in the latter two cases $b_{r\mathrm{b}}$ is required to exceed a certain lower bound (which is at least $2/\sqrt{3}$; see Section 5.2) to satisfy the wind launching condition. It is also worth noting in this connection that, even if the magnetic field at the disc surface is not bent strongly enough to satisfy the wind launching requirement, vertical magnetic angular-momentum transport along a large-scale field that threads the disc could potentially still take place by other means, such as magnetic braking (see footnote 1).

By combining the wind-launching and wind-loading constraints (the second and third inequalities, respectively, in Tables 1 and 3) and using the expression for $\tilde{h}$ in the fifth column of Tables 2 and 4, one finds that $\tilde{h} < 1$, i.e. that the vertical confinement of the disc is primarily magnetic [due to the vertical gradient of $(B_r^2 + B_\phi^2)/8\pi$] rather than tidal for all the cases in the Hall and Ohm regimes. This result, which was previously shown by WK93 to apply to ambipolar diffusion-dominated discs, is corroborated by the full solutions presented in Paper II. Predominantly magnetic confinement is thus seen to be a generic property of our wind-driving disc model. The generality of this result was, however, questioned by Ferreira (1997), who suggested that it might be a consequence of the simplification $\rho v_z = \mathrm{const}$ adopted in our treatment of the mass

[16] Such configurations were later found to arise naturally in certain models of disc formation from the collapse of rotating molecular cloud cores (see Krasnopolsky & Königl 2002).

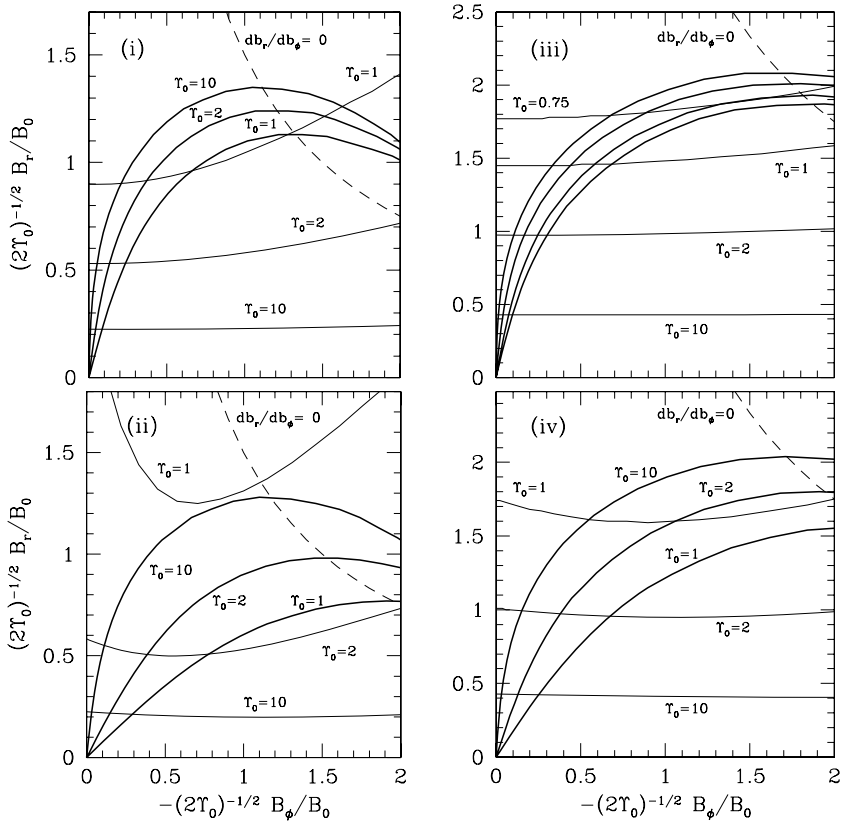

Figure 2. Same as Fig. 1, but in the limit where the Hall diffusivity dominates. The four panels correspond to Cases (*i*) through (*iv*) in Table 1. Note that, as in the ambipolar diffusion regime shown in Fig. 1, physically viable solutions satisfy $\Upsilon_0 \gtrsim 1$ also in each of the Hall sub-regimes.

conservation relation. In addressing this question, it is interesting to note that the inequality $\tilde{h} < 1$ was inferred in this paper already on the basis of the hydrostatic approximation, which does not make use of the continuity equation. On the other hand, our argument involved an estimate of $\tilde{z}_b$, the normalized height of the disc surface, which corresponds to a disc region where the hydrostatic approximation may no longer be accurate. A definitive resolution of this issue would require using a more elaborate model in which the above simplification is not made.

The wind-loading and energy dissipation constraints (the third and fourth inequalities, respectively, in Tables 1 and 3) provide lower and upper bounds, respectively, on the radial velocity parameter ϵ. The lower bound reflects the fact that the height of the disc surface scales as ϵ whereas the scaleheight scales as $1/\epsilon$, so that $\tilde{z}_b/\tilde{h}$, which is required to be >1, scales as ϵ^2 (see the fifth and sixth columns in Tables 2 and 4). The upper bound is a consequence of the fact that both the electric field and the current density scale as ϵ, so that the Joule dissipation (which scales as ϵ^2 – see the seventh column in Tables 2 and 4) might exceed the rate of gravitational energy release ($\propto \epsilon$) if the inflow speed were too high. The solutions presented in Paper II have values of ϵ in the range ∼0.3–1. With these parameters, one infers a nominal emptying time $\lesssim 10^4$ yr for a representative protostellar disc, which is consistent with the mean duration of the earliest (Class 0) phase of protostellar evolution but is very much shorter than the total age of accreting protostars. This is the essence of the 'short evolution time' critique of pure-wind angular-momentum transport models of protostellar discs, which has led to the argument that alternative angular-momentum transport mechanisms must dominate in such systems (e.g. Shu et al. 2008).[17] Note, however, that even if a centrifugally driven wind does not control the overall evolution of the disc throughout its lifetime, it might still dominate the angular momentum transport in regions of the disc from which strong outflows are launched, which may be especially pertinent during the FU Orionis-type rapid accretion episodes that are thought to account for most of the mass deposition on to low-mass protostars (e.g. Calvet et al. 2000). Furthermore, wind-mediated angular momentum transport could in principle also contribute in regions where a radial transport mechanism dominates (see Salmeron et al. 2007). It is also worth noting that significantly lower mean inflow speeds could be attained in more realistic, vertically stratified wind-driving disc models (e.g. Königl & Salmeron 2009), and in particular in *weakly coupled* discs (see Li 1996; Wardle 1997). Further work is, however, required to determine the extent to which this effect would increase the predicted disc evolution time.

We have been careful to use the absolute values of β_{i0} and β_{e0} in delineating the various sub-regimes in the Hall and Ohm domains in view of the fact that our definition (equation 4) of the Hall parameters has an explicit dependence on the magnetic field polarity and thus allows them to have both positive and negative values. However, in our table entries for the Hall Cases (*ii*) and (*iv*) and for the Ohm Case (*iii*) we implicitly treated the ion and electron Hall parameters as *positive* quantities. This can be readily justified by

[17] These alternative mechanisms potentially include vertical transport along a large-scale open magnetic field by means other than the steady wind that has been the focus of our discussion (see footnote 1).

observing that these cases correspond to $|\beta|$ being $>2\psi$ and taking note of the inequality $\beta > -2\psi$ (equation 108) that all viable solutions must obey. These two inequalities can be simultaneously satisfied only if $\beta > 0$. In other words, for these parameter sub-regimes a self-consistent wind-driving disc solution can be obtained only if the field has a positive polarity but not if $\mathrm{sgn}\{B_z\} < 0$. The sensitivity to the field polarity reflects the explicit dependence on the Hall conductivity in these cases (see Sections 2.1 and 5.6) and is a specific prediction of our model that is checked in the numerical work presented in Paper II. We emphasize that our discussion here concerns the nature of certain sub-regimes, in which *only* solutions with $\beta > 0$ are predicted to exist. This property is distinct from the dependence of wind-driving wind solutions on the field polarity in other parameter sub-regimes in which *both* positive and negative values of β are allowed but in which changing the sign of β modifies the behaviour of the solution (see WK93). An example of the latter dependence is given in Paper II for the Hall Case (*iii*), which admits β values in the range $-\psi/2 < \beta < 2\psi$ (see equation 114).

Our analysis has concentrated on discs with a charged-particle composition that can be represented as a two-component plasma consisting of electrons and comparatively massive ions, with the parameter q (equation 7) being $\ll 1$. This composition is appropriate to relatively low-density disc regions or even to denser zones that do not contain dust (see footnote 5). Weakly ionized disc regions that have densities $\gtrsim 10^{-13}\,\mathrm{g\,cm^{-3}}$ and contain dust may be better approximated by a two-component, $q = 1$ plasma corresponding to oppositely charged grains of equal mass (see Section 2.1). In this case the Hall regime is not present (see equation 95) and the parameter space of viable solutions consists of only two regimes (ambipolar diffusion and Ohm). One can readily verify that, under these circumstances, the Ohm domain contains only two sub-regimes, the analogues of the Ohm Cases (*i*) and (*ii*) for a $q \ll 1$ plasma.[18] This finding is not surprising in view of the fact (see Section 5.6) that the Ohm Case (*iii*) for a $q \ll 1$ plasma arises from the Hall-current term in Ohm's law, which is missing when $q = 1$.

The viability constraints that we derived on diffusive accretion discs in which the entire excess angular momentum is transported by a centrifugally driven wind can be useful also for generalizing the model to incorporate other modes of angular momentum transport. In particular, one can argue (see Salmeron et al. 2007) that radial angular-momentum transport through MRI-induced turbulence could operate at disc locations where the sub-Keplerian rotation constraint (expressed by the first inequality in Tables 1 and 3, in which the various parameters are taken to have their *local*, density-dependent values) is violated. For example, in the ambipolar diffusion case (as well as in the Hall Cases *i* and *iii* and the Ohm Cases *i* and *ii*) this corresponds to $2\Upsilon a^2 \propto \rho_\mathrm{i}/\rho$ being <1. As this quantity is expected to increase with height on account of the increase in the fractional ionization of the gas on going away from the disc mid-plane, one can envision a situation in which $2\Upsilon a^2$ is <1 (with both radial and vertical angular-momentum transport taking place) in the vicinity of the mid-plane but becomes >1 (with only vertical transfer into a wind remaining relevant) closer to the disc surfaces. This criterion can be employed for constructing a 'hybrid' disc model in which both vertical and radial angular momentum transport take place (through a large-scale, ordered magnetic field and a small-scale, disordered field, respectively; see Salmeron et al. 2007 for details).

[18] Note from equations (95)-(97) that the parameter $\psi = \Upsilon_0$ always appears in the conductivity tensor in the combination $(1 + q)\,\psi$. Therefore, the parameter Υ_0 in the expressions for the $q \ll 1$ Cases (*i*) and (*ii*) in Tables 3 and 4 is replaced by $2\Upsilon_0$ in the corresponding expressions for $q = 1$.

7 CONCLUSION

We have investigated a protostellar accretion disc model in which the dominant angular momentum transport mechanism is a centrifugally driven wind launched along a large-scale, ordered magnetic field that threads the disc. The basic assumptions we adopted are the same as those of the radially localized disc model constructed by WK93, and our main purpose has been to extend the analysis presented in that paper, which focused on discs in which ambipolar diffusion dominates the magnetic diffusivity inside the disc, to a general diffusivity regime. In particular, we included also the Hall and Ohm diffusivities, which are relevant to higher-density disc regions than those covered by the WK93 treatment. We employed a tensor-conductivity scheme that, in conjunction with an ionization-balance calculation, can be used to determine realistic vertical conductivity profiles for protostellar discs in the context of this model. However, in this paper and its follow-up (Paper II), we adopt a simpler treatment and assume that the three model parameters that are needed to identify the distinct solution regimes for an ion–electron plasma remain constant with height in the disc. The three variables employed for this purpose in the current paper are the electron and ion Hall parameters (β_e and β_i, respectively, with $|\beta_\mathrm{i}| \ll |\beta_\mathrm{e}|$) and the neutral–ion coupling parameter Υ (equation 82). In Paper II we use instead two independent ratios of the conductivity-tensor components as well as the Elsasser number Λ [see items (*iii*) and (*iv*) in Section 3.13].

We determined the parameter regimes where physically viable disc solutions could be found by employing the hydrostatic approximation and imposing the following requirements (originally applied in the ambipolar diffusion regime by WK93 and Königl 1997) on 'strongly coupled' systems (discs in which the magnetic field is dynamically well coupled to the bulk of the matter already at the mid-plane): (i) the disc (in contradistinction to the wind) rotates at sub-Keplerian speeds; (ii) a wind launching condition (which yields a lower limit on B_r/B_z) is satisfied at the disc surface; (iii) most of the disc material is located below the wind-launching region and (iv) the rate of Joule dissipation does not exceed the rate of gravitational energy release in the disc. Our main results can be summarized as follows.

(i) In addition to the ambipolar diffusion regime considered in WK93, there are four distinct sub-regimes in the Hall diffusion-dominated parameter domain and three distinct sub-regimes in the Ohm domain. (A fourth potential Ohm sub-regime was found not to be consistent with the wind-launching requirement.) The four Hall sub-regimes naturally divide into two ambipolar diffusion-like and two Ohm-like parameter regions: in the former pair one of the sub-regimes has the same structural properties as the ambipolar diffusion regime, whereas in the latter pair the solution characteristics of one of the sub-regimes are identical to those of one of the Ohm sub-regimes. In the case (not treated in detail in this paper) of a high-density disc plasma dominated by oppositely charged grains of equal mass, only an ambipolar diffusion regime and an Ohm regime (with two sub-regimes corresponding to our Ohm Cases *i* and *ii*) are present.

(ii) All viable solutions, irrespective of the diffusivity regime, are found to satisfy $\Upsilon \gtrsim 1$. The physical requirement expressed by this condition, that the neutral–ion momentum exchange time be shorter

than the disc orbital time, is thus indicated to be a fundamental constraint on wind-driving discs of this type.

(iii) Viable solutions are also characterized by the parameters a_0 (mid-plane Alfvén-to-sound speed ratio) and ϵ (mid-plane inflow-to-sound speed ratio) being $\lesssim 1$. However, weakly coupled discs, characterized by values of Λ_0 (the mid-plane value of the Elsasser number; see Section 3.13) that are $\ll 1$, could have $a_0 \ll 1$ and $\epsilon \ll 1$. In such systems a significant bending of the magnetic field away from the rotation axis (required for driving a centrifugally driven wind) takes place only above some finite height in the disc, although vertical angular momentum transport along the large-scale field typically occurs already at lower elevations. Although our analysis does not directly apply to weakly coupled discs, our results should be useful for understanding the basic qualitative aspects of their behaviour.

(iv) The wind-launching and wind-loading conditions [the aforementioned requirements (*ii*) and (*iii*), respectively] together imply that magnetic squeezing (by the gradient of the magnetic pressure force associated with the transverse field components B_r and B_ϕ) dominates the gravitational tidal compression of the disc. A more elaborate model is, however, needed to verify the full generality of this result.

(v) The transverse magnetic field at the disc surface is dominated by the radial component in all the Hall parameter sub-regimes (including their 'twins' in the ambipolar-diffusion and Ohm domains), and by the azimuthal component in the remaining two Ohm sub-regimes. However, even in the latter two cases the poloidal surface magnetic field must be sufficiently strongly bent to satisfy the wind launching requirement.

Centrifugally driven winds are not the only means of vertical angular momentum transport in a protostellar disc (magnetic braking is an example of another option), and there are also alternative mechanisms that involve radial transport along the plane of the disc. It is nevertheless instructive to investigate the limiting case in which wind transport dominates at a given radius in view of the ubiquity of energetic outflows in protostellar systems and the inferred association of disc winds with FU Orionis-type high-accretion-rate events. The constraints considered in our model can also be useful for identifying the parameter regimes where other mechanisms (such as MRI-induced turbulence) are likely to operate, possibly even at the same radial location as wind-mediated angular momentum transport (Salmeron et al. 2007).

The parameter regimes that we identified were determined under the assumption that the values of the parameters used in the classification scheme did not vary with height in the disc. This approximation becomes less accurate as one moves from the ambipolar-diffusion regime to the Hall regime and then (at even higher disc densities and column densities) to the Ohm regime. In particular, in the latter case it can be expected that if a real disc could be described as being in this regime at the mid-plane then it would transit to the Hall regime further up and would likely be ambipolar diffusion-dominated at the surface. For this reason (and also because wind-driving discs might not be massive enough to harbour an Ohm regime within their weakly ionized zones) we have emphasized the Hall regime in our discussion and do not consider the Ohm domain in Paper II. However, our findings for the Ohm regime could still be applicable to the innermost, collisionally ionized regions of protostellar discs (and possibly also to disc regions participating in an FU Orionis-type outburst), in which an anomalous ohmic resistivity might dominate.

The actual parameter regime that characterizes a given section of an accretion disc of the type that we have modelled will be determined by the global magnetic flux distribution, the density structure (which depends in part on the mass accretion rate) and the ionization profile (which depends in part on the nature of the ionization sources as well as on the disc composition). It is conceivable that some of the sub-regimes that we have identified are not commonly realized in nature or that they correspond to unstable configurations. More insight into these questions would likely emerge from comparisons with observations as well as from additional analytic and numerical work. Our study has, however, indicated that, if such wind-driving accretion flows are indeed present in real protostellar systems, they will exhibit certain generic properties (including good neutral–ion coupling, subthermal Alfvén and inflow speeds and magnetic squeezing within the field-line bending region) irrespective of the particular parameter regime to which they correspond.

ACKNOWLEDGMENTS

We thank the reviewer for helping us improve the presentation of this paper. This research was supported in part by NASA Theoretical Astrophysics Programme grant NNG04G178G (AK and RS), by NSF grant AST-0908184 (AK) and by the Australian Research Council grants DP0344961 and DP0881066 (RS and MW).

REFERENCES

Alexander R. D., Clarke C. J., Pringle J. E., 2005, MNRAS, 358, 283
Balbus S. A., Hawley J. F., 1998, Rev. Mod. Phys., 70, 1
Balbus S. A., Terquem C., 2001, ApJ, 552, 235
Bally J., Reipurth B., Davis C. J., 2007, in Reipurth B., Jewitt D., Keil K., eds, Protostars & Planets V. Univ. Arizona Press, Tucson, p. 215
Bell K. R., Lin D. N. C., 1994, ApJ, 427, 987
Blaes O. M., Balbus S. A., 1994, ApJ, 421, 163
Blandford R. D., Payne D. G., 1982, MNRAS, 199, 883 (BP82)
Brandenburg A., Nordlund A., Stein R. F., Torkelsson U., 1995, ApJ, 446, 741
Calvet N., Hartmann L., Strom S. E., 2000, in Mannings V. G., Boss A. P., Russell S., eds, Protostars & Planets IV. Univ. Arizona Press, Tucson, p. 377
Calvet N., Briceño C., Hernández J., Hoyer S., Hartmann L., Sicilia-Aguilar A., Megeath S. T., D'Alessio P., 2005, AJ, 129, 935
Casse F., Ferreira J., 2000, ApJ, 353, 1115
Casse F., Keppens R., 2002, ApJ, 581, 988
Ciolek G. E., Mouschovias T. Ch., 1993, ApJ, 418, 774
Corcoran M., Ray T. P., 1998, A&A, 331, 147
Cowling T. G., 1976, Magnetohydrodynamics. Adam Hilger, Bristol
D'Alessio P., Calvet N., Hartmann L., Franco-Hernandez R., Servin H., 2006, ApJ, 638, 314
Desch S. J., 2004, ApJ, 608, 509
Draine B. T., Roberge W. G., Dalgarno A., 1983, ApJ, 264, 485
Dullemond C. P., Dominik C., 2004, A&A, 421, 1075
Ferreira J., 1997, A&A, 319, 340
Fleming T., Stone J. M., 2003, ApJ, 585, 908
Gammie C. F., 1996, ApJ, 457, 355
Gammie C. F., 1999, in Sellwood J. A., Goodman J., eds, ASP Conf. Ser. Vol. 160, Astrophysical Discs. Astron. Soc. Pac., San Francisco, p. 122
Girart J. M., Rao R., Marrone D. P., 2006, Sci, 313, 812
Glassgold A. E., Feigelson E. D., Montmerle T., Wolk S., 2005, in Krot A., Scott E. R. D., Reipurth B., eds, ASP Conf. Ser. Vol. 341, Chondrites and the Protoplanetary disk. Astron. Soc. Pac., San Francisco, p. 165
Hartigan P., Edwards S., Ghandour L., 1995, ApJ, 452, 736
Hartmann L., Kenyon S. J., 1996, ARA&A, 34, 207
Hawley J. F., Stone J. M., 1998, ApJ, 501, 758

Hayashi C., 1981, Prog. Theor. Phys. Suppl., 70, 35
Igea J., Glassgold A. E., 1999, ApJ, 518, 848
Kirby L., 2009, ApJ, 694, 1056
Königl A., 1989, ApJ, 342, 208
Königl A., 1997, in Wickramasinghe D. T., Bicknell G. V., Ferrario L., eds, Proc. IAU Colloq. 163, ASP Conf. Ser. Vol. 121, Accretion Phenomena and Related Outflows. Astron. Soc. Pac., San Francisco, p. 551
Königl A., Pudritz R. E., 2000, in Mannings V. G., Boss A. P., Russell S. eds, Protostars & Planets IV. Univ. Arizona Press, Tucson, p. 759
Königl A., Salmeron R., 2009, in Garcia P. J. V., ed., Physical Processes in Circumstellar Disks around Young Stars. Univ. Chicago Press, Chicago, in press
Krasnopolsky R., Königl A., 2002, ApJ, 580, 987
Kuwabara T., Shibata K., Kudoh T., Matsumoto R., 2005, ApJ, 621, 921
Levreault R. M., 1988, ApJ, 330, 897
Li Z.-Y., 1995, ApJ, 444, 848
Li Z.-Y., 1996, ApJ, 465, 855
Lovelace R. V. E., Romanova M. M., Newman W. I., 1994, ApJ, 437, 136
Lubow S. H., Papaloizou J. C. B., Pringle J. E., 1994, MNRAS, 267, 235
Mac Low M. M., Norman M. L., Königl A., Wardle M., 1995, ApJ, 442, 726
Meliani Z., Casse F., Sauty C., 2006, A&A, 460, 1
Mitchner M., Kruger C. H. Jr., 1973, Partially Ionized Gases. Wiley-Interscience, New York
Mohanty S., Jayawardhana R., Basri G., 2005, ApJ, 626, 498
Nakagawa Y., Nakazawa K., Hayashi C., 1981, Icarus, 45, 517
Nakano T., Nishi R., Umebayashi T., 2002, ApJ, 573, 199
Neufeld D. A., Hollenbach D. J., 1994, ApJ, 428, 170
Ogilvie G. I., Livio M., 2001, ApJ, 553, 158
Pudritz R. E., Ouyed R., Fendt Ch., Brandenburg A., 2007, in Reipurth B., Jewitt D., Keil K., eds, Protostars & Planets V. Univ. Arizona Press, Tucson, p. 277
Ray T., Dougados C., Bacciotti F., Eislöffel J., Chrysostomou A., 2007, in Reipurth B., Jewitt D., Keil K., eds, Protostars & Planets V. Univ. Arizona Press, Tucson, p. 231
Salmeron R., Wardle M., 2003, MNRAS, 345, 992
Salmeron R., Wardle M., 2005, MNRAS, 361, 45
Salmeron R., Wardle M., 2008, MNRAS, 388, 1223
Salmeron R., Königl A., Wardle M., 2007, MNRAS, 375, 177
Sano T., Stone J. M., 2002a, ApJ, 570, 314
Sano T., Stone J. M., 2002b, ApJ, 577, 534
Sano T., Inutsuka S. I., Turner N. J., Stone J. M., 2004, ApJ, 605, 321
Schleuning D. A., 1998, ApJ, 493, 811
Semenov D., Wiebe D., Henning Th., 2004, A&A, 417, 93
Shu F. H., Adams F. C., Lizano S., 1987, ARA&A, 25, 23
Shu F. H., Lizano S., Galli D., Cai M. J., Mohanty S., 2008, ApJ, 682, L121
Takeuchi T., Lin D. N. C., 2002, ApJ, 581, 1344
Tassis K., Mouschovias T. Ch., 2005, ApJ, 618, 783
Turner N. J., Sano T., Dziourkevitch N., 2007, ApJ, 659, 729
Umebayashi T., Nakano T., 1981, PASJ, 33, 617
Umebayashi T., Nakano T., 1990, MNRAS, 243, 103
Wardle M., 1997, in Wickramasinghe D. T., Bicknell G. V., Ferrario L., eds, Proc. IAU Colloq. 163, ASP Conf. Ser. Vol. 121, Accretion Phenomena and Related Outflows. Astron. Soc. Pac., San Francisco, p. 561
Wardle M., 1999, MNRAS, 307, 849
Wardle M., 2007, Ap&SS, 311, 35
Wardle M., Königl A., 1993, ApJ, 410, 218 (WK93)
Wardle M., Ng C., 1999, MNRAS, 303, 239
Zanni C., Ferrari A., Rosner R., Bodo G., Massaglia S., 2007, A&A, 469, 811

APPENDIX A: THE $\epsilon_B \approx 0$ APPROXIMATION

In their consideration of a weakly ionized disc containing a two-component plasma, WK93 noted the qualitative similarity of solutions characterized by the same value of the parameter combination $(\epsilon - \epsilon_B)$. They attributed this result to the fact that the only change in the underlying system of equations introduced by switching to a reference frame that moves with the radial velocity $v_{Br0} = -\epsilon_B c_s$ of the poloidal flux surfaces involves the magnitude of the torque that is required to remove the excess angular momentum, so that all radial-velocity terms (except in the angular momentum equation, which remains unchanged) are modified simply by subtracting v_{Br0} from the radial velocity component. We appealed to this result in Section 3.13 to motivate setting $\epsilon_B = 0$ in our analysis.

One could, however, question this approach on the basis of the following consideration. Starting from Ohm's law in the form $\boldsymbol{E}' = \boldsymbol{E} + \boldsymbol{v} \times \boldsymbol{B}/c = (4\pi/c^2)\, \boldsymbol{\eta} \cdot \boldsymbol{J}$, where $\boldsymbol{\eta}$ is the diffusivity tensor, we rewrite it in terms of normalized quantities as

$$\begin{pmatrix} w_{Br0} - w_r \\ \\ w_{B\phi 0} - w_\phi \end{pmatrix} = \begin{pmatrix} \tilde{\eta}_H & -\tilde{\eta}_P \\ \\ \tilde{\eta}_P & \tilde{\eta}_H \end{pmatrix} \begin{pmatrix} 0.5\, w_r \\ \\ 2\, w_\phi \end{pmatrix}, \tag{A1}$$

where $\tilde{\eta}_P = \tilde{\eta}_O + \tilde{\eta}_A$ and where $\tilde{\eta}_O$, $\tilde{\eta}_H$ and $\tilde{\eta}_A$ are obtained by multiplying the expressions in equations (29)–(31), respectively, by $1/h_T c_s a_0^2$. We have also written $w_{Br0} \equiv v_{Br0}/c_s = w_{E\phi 0}$ and $w_{B\phi 0} \equiv r(\Omega_{B0} - \Omega_K)/c_s = -w_{Er0}$ for the normalized mid-plane radial and azimuthal velocities, respectively, of the poloidal flux surfaces. By inspecting equation (A.1) one may be induced to infer that, since the off-diagonal terms of the diffusivity tensor dominate in the ambipolar-diffusion and Ohm regimes whereas the diagonal terms are dominant in the Hall limit, one should retain the latter terms when considering the Hall regime and the former terms when treating the other limits. This inference could be carried over to the analysis of equation (98) in the text, in which the matrix is related to the inverse of the matrix that appears in equation (A1). Specifically, specializing to the mid-plane (where $b_r = b_\phi = 0$) and assuming $q \ll 1$ for simplicity, one can use equations (95)–(97) to deduce that $A_1 = -A_4 \propto \sigma_P/\sigma_\perp$ (with the factor $q\beta^2$ in equations 99 and 102 representing the ratio η_O/η_A). One can similarly deduce that the term β in the expressions for A_2 and A_3 is $\propto \sigma_H/\sigma_\perp$ (with the term involving ψ in equations 100 and 101 arising from the advective contribution to the electric field). Adopting the above reasoning, it would appear that one should retain the diagonal terms A_1 and A_4 in the ambipolar-diffusion and Ohm regimes and the off-diagonal terms A_2 and A_3 in the Hall limit. However, this procedure cannot be implemented if one sets ϵ_B to be identically zero in equation (98), as we have done in our analysis, which casts doubt on the validity of the approach followed in the text.

In addressing this question, it is important to keep in mind the basic attributes of the system that we wish to model. We are primarily interested in the quasi-steady behaviour of a disc in which mass and poloidal magnetic flux that were originally part of a large-scale equilibrium configuration of a molecular cloud core are carried in by the accretion flow. In this picture, the accretion is enabled in large measure by the vertical magnetic transport of angular momentum, and the inward motion of the matter is, in turn, responsible for the radial transport of the field lines (which, however, generally lag behind the matter because of the disc's diffusivity). The vertical magnetic transport of angular momentum implies that $J_r B_z > 0$ and hence that $w_r < 0$ (see equation 92), whereas the inward bending of the magnetic field lines by the inflowing gas implies that $J_\phi B_z > 0$ and hence that $w_\phi < 0$ (see equation 91). The fact that the motion of the field lines is controlled by that of the gas implies that $w_{B\phi} = -w_{Er}$ would also be <0 (see Section 3.12). In a similar vein, we expect the radial velocity of the poloidal field lines (described by

the parameter $w_{\mathrm{B}r0} = -\epsilon_{\mathrm{B}}$) to satisfy $w_{r0} \leq w_{\mathrm{B}r0}$ (or, equivalently, $\epsilon_{\mathrm{B}} \leq \epsilon$).[19]

We now proceed to examine the consequences of the alternative formulation outlined above in light of the just-discussed constraints. To this end, we substitute for j_{r0} and $j_{\phi 0}$ in equation (98) from equations (92) and (91), respectively, to obtain

$$A_1\, w_{\mathrm{E}r0} + A_2\, \epsilon_{_{\mathrm{B}}} = \frac{K\epsilon}{2\psi}, \tag{A2}$$

$$A_3\, w_{\mathrm{E}r0} + A_4\, \epsilon_{\mathrm{B}} = -\frac{2K\, w_{\phi 0}}{\psi}. \tag{A3}$$

In the ambipolar-diffusion and Ohm regimes we retain only the A_1 and A_4 terms. In the ambipolar diffusion limit $A_1 = -A_4 \approx 1$ and $K \approx 1 + \psi^2 \approx \psi^2$ (since ψ is equal in this case to the mid-plane value of the neutral–field coupling parameter Λ, which is expected to be >1), so equation (A3) implies $\epsilon_{\mathrm{B}} = 2\psi\, w_{\phi 0} < 0$, which is inconsistent with our expectation that $\epsilon_B \geq 0$. Similarly, in the Ohm limit $A_1 = -A_4 \approx q\beta^2$ and $K \approx q\beta^2 + \psi^2$, so equation (A.3) implies $\epsilon_{\mathrm{B}} = 2\,(\psi/q\beta^2 + q\beta^2/\psi)\, w_{\phi 0}$, which is again inferred to be <0, contrary to our physical expectation. In a similar vein, we retain only the A_2 and A_3 terms in the Hall regime. Using equations (100) and (101) and focusing on the case $q \ll 1$, we infer from equations (A2) and (A3) that

$$\frac{\epsilon_{\mathrm{B}}}{\epsilon} = \frac{1 + \frac{5}{2}\frac{\psi}{\beta} + \left(\frac{\beta}{\psi}\right)^2}{1 + \frac{2\beta}{\psi}} \tag{A4}$$

and

$$\frac{w_{\mathrm{E}r0}}{-w_{\phi 0}} = \frac{1 + \frac{5}{2}\frac{\psi}{\beta} + \left(\frac{\beta}{\psi}\right)^2}{1 + \frac{\beta}{2\psi}}. \tag{A5}$$

One can readily verify that equations (A4) and (A5) cannot be simultaneously satisfied while also respecting the constraints $0 \leq \epsilon_{\mathrm{B}}/\epsilon \leq 1$ and $w_{\mathrm{E}r0}/w_{\phi 0} < 0$. These arguments indicate that a formulation based simply on the dominant terms in the conductivity tensor is not physically self-consistent for the problem under consideration.

In contrast, one can verify that the formulation adopted in the text is self-consistent – in the sense that the neglected terms in equations (A2) and (A3) never come to dominate the ones that were retained – under the assumption $\epsilon_{\mathrm{B}}/\epsilon \leq 1$. In particular, using the expression (113) for $w_{\mathrm{E}r0}$ and equations (99)–(102), it is straightforward to ascertain that the ratios $|A_2\epsilon_{\mathrm{B}}/A_1 w_{\mathrm{E}r0}|$ and $|A_4\epsilon_{\mathrm{B}}/A_3 w_{\mathrm{E}r0}|$ remain ≤ 1 in this case for all the viable-solution parameter regimes identified in Sections 4 and 5.

This paper has been typeset from a TEX/LATEX file prepared by the author.

[19] It is conceivable that ϵ_{B} and ϵ could have opposite signs, but such a situation would likely only arise in the context of a localized, time-dependent phenomenon. An example of this possibility is provided by the cyclical behaviour exhibited by the core-collapse solutions of Tassis & Mouschovias (2005) near the boundary of their computational 'central sink.' This behaviour is indeed localized (in both space and time) and clearly does not correspond to the global, quasi-steady accretion process analyzed in this paper.